Inorg. Chem. **2007**, *46*, 3916–3933

Synthesis and Spectroscopic Characterization of Copper(II)–Nitrito Complexes with Hydrotris(pyrazolyl)borate and Related Coligands

Nicolai Lehnert,*,† Ursula Cornelissen,‡ Frank Neese,*,§ Tetsuya Ono,|| Yuki Noguchi,|| Ken-ichi Okamoto,|| and Kiyoshi Fujisawa*,||

Department of Chemistry, The University of Michigan, 930 North University, Ann Arbor, Michigan 48109, Institut für Anorganische Chemie, Christian-Albrechts-Universität Kiel, Olshausenstrasse 40, D-24098 Kiel, Germany, Institut für Physikalische and Theoretische Chemie, Rheinische Friedrich-Wilhelms-Universität Bonn, Wegelerstrasse 12, 53115 Bonn, Germany, and Graduate School of Pure and Applied Sciences, Department of Chemistry, University of Tsukuba, Tsukuba 305-8571, Japan

Received October 10, 2006

This study focuses on the geometric (molecular) structures, spectroscopic properties, and electronic structures of copper(II)–nitrito complexes as a function of second coordination sphere effects using a set of closely related coligands. With anionic hydrotris(pyrazolyl)borate ligands, one nitrite is bound to copper(II). Depending on the steric demand of the coligand, the coordination mode is either symmetric or asymmetric bidentate, which leads to different ground states of the resulting complexes as evident from EPR spectroscopy. The vibrational spectra of these compounds are assigned using isotope substitution and DFT calculations. The results demonstrate that ν_{sym}(N–O) occurs at higher energy than ν_{asym}(N–O), which is different from the literature assignments for related compounds. UV–vis absorption and MCD spectra are presented and analyzed with the help of TD-DFT calculations. The principal binding modes of nitrite to Cu(II) and Cu(I) are also investigated applying DFT. Using a neutral tris(pyrazolyl)methane ligand, two nitrite ligands are bound to copper. In this case, a very unusual binding mode is observed where one nitrite is η^1-O and the other one is η^1-N bound. This allows to study the properties of coordinated nitrite as a function of binding mode in one complex. The N-coordination mode is easily identified from vibrational spectroscopy, where N-bound nitrite shows a large shift of ν_{asym}(N–O) to >1400 cm^{-1}, which is a unique spectroscopic feature. The optical spectra of this compound exhibit an intense band around 300 nm, which might be attributable to a nitrite to Cu(II) CT transition. Finally, using a bidentate neutral bis(pyrazolyl)methane ligand, two η^1-O coordinated nitrite ligands are observed. The vibrational and optical (UV–vis and MCD) spectra of this compound are presented and analyzed.

Introduction

Copper(II)−nitrite complexes are relevant for the copper nitrite reductase (CuNIR) class of enzymes that are part of the biological denitrification process.[1−3] These enzymes are homotrimers where the catalytically active type 2 centers are located at each of the interfaces of two subunits of the enzyme. In the oxidized form, the type 2 centers are tetrahedrally coordinated by three histidines and a water molecule.[4] The fact that the type 2 centers are the location of catalytic activity is evident from type 2 depleted enzyme, which does not show any NIR activity.[5] Correspondingly, ENDOR, EXAFS, and X-ray crystallographic studies have shown that nitrite binds to the type 2 center of oxidized (inactive) enzyme. The observed coordination mode is asymmetric η^2-O,O (cf. Chart 1) corresponding to the

* To whom correspondence should be addressed. E-mail: lehnertn@umich.edu (N.L.); neese@xthch.uni-bonn.de (F.N.); kiyoshif@staff.chem.tsukuba.ac.jp (K.F.).
† The University of Michigan.
‡ Christian-Albrechts-Universität Kiel.
§ Rheinische Friedrich-Wilhelms-Universität Bonn.
|| University of Tsukuba.

(1) (a) Ferguson, S. J. *Curr. Opin. Chem. Biol.* **1998**, *2*, 182−193. (b) Richardson, D. J.; Watmough, N. J. *Curr. Opin. Chem. Biol.* **1999**, *3*, 207−219. (c) Moura, I.; Moura, J. J. G. *Curr. Opin. Chem. Biol.* **2001**, *5*, 168−175.
(2) (a) Wasser, I. M.; de Vries, S.; Moënne-Loccoz, P.; Schröder, I.; Karlin, K. D. *Chem. Rev.* **2002**, *102*, 1201−1234. (b) Suzuki, S.; Kataoka, K.; Yamaguchi, K. *Acc Chem. Res.*, **2000**, *33*, 728−735.
(3) Averill, B. A. *Chem. Rev.* **1996**, *96*, 2951−2964.

10.1021/ic0619355 CCC: $37.00
Published on Web 04/21/2007

Chart 1. Different Binding Modes of Nitrite

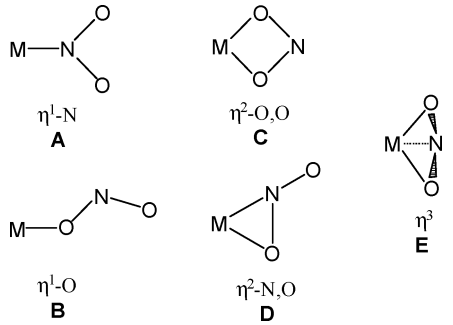

formation of a Cu(II)−nitrito complex.[4b,d,6,7] Note that η^2-O,O bonding is also observed for almost all corresponding copper(II) model complexes (vide infra). Two different molecular mechanisms have been proposed for CuNIR. Initially, Averill and co-workers postulated a molecular mechanism similar to that of heme cd_1 nitrite reductase,[3] where nitrite binds to the reduced Cu(I) form of the type 2 center via its N-atom. On the basis of crystallographic results revealing potential hydrogen bonding amino acid residues in close proximity of the type 2 center, an alternative mechanism has been proposed by Suzuki and co-workers.[8] In this case, nitrite binding is proposed to the oxidized copper(II) form, i.e., the initial electron transfer takes place after nitrite coordination. The obtained Cu(II)−nitrito species is stabilized by hydrogen bridges to protein side chains. This form has also been structurally characterized as described above. This mechanism is supported by recent studies where it was shown that nitrite coordination to the oxidized copper type 2 center increases the redox potential of the site, which would trigger electron transfer.[9] On the other hand, site-directed mutagenesis experiments of Asp92 to a nonionizable Asn residue leads to a mutant that has 60% activity of the wild-type enzyme.[10] Hence, this questions the critical role of Asp92 in the proposed mechanism. Finally, mononuclear Cu(I)−nitrite model complexes using the TACN coligand (1,4,7-triazacyclononane) studied by Tolman and co-workers show N-coordinated nitrite, which, upon addition of acid, generate NO and water.[11] From crystallography, the observed Cu−N(nitrite) distance is 1.90 Å.[11b] These findings again support the mechanism proposed by Averill (see also ref 12). However, new crystallographic results have surprisingly indicated different binding modes of nitrite and nitric oxide to the copper type 2 center in CuNIR than previously assumed.[13] In contrast to the model complex studies, the nitrite ion is bound with its oxygen atoms to the copper(I) type 2 center, which is in agreement with the Suzuki mechanism. However, the binding mode of nitrite seems to be tridentate including a weak Cu−N interaction. In addition, the crystal structure of the resulting formal Cu(II)−NO enzyme−product complex was also obtained showing an unprecedented side-on coordination mode of nitric oxide to the copper(II) center.

Based on these results, the relevant species that need to be considered in model complex studies are Cu(II)−nitrite, Cu(I)−nitrite, Cu(I)−NO, and Cu(II)−NO compounds. In general, of these four species only the Cu(II)−nitrite complexes are stable. Hence, a number of corresponding model complexes has been synthesized as listed in ref 2. These compounds show mono- or bidentate coordination of nitrite to the copper center via its oxygen atom(s). This corresponds to the binding modes B and C in Chart 1. A few Cu(II)−nitrito complexes with hydrotris(pyrazolyl)borate ligands have been characterized by X-ray crystallography showing either a symmetric or asymmetric η^2-O,O coordination mode of the NO_2^- ligand depending on the pyrazolyl substituents.[14,15] Importantly, these compounds do not support nitric oxide formation from nitrite. Cu(II)−nitrito complexes with tris(2-pyridylmethyl)amine (TMPA) as coligand show an interesting solvent-induced interconversion between η^1-N bound nitrite obtained when recrystallized in water, whereas usage of methanol for recrystallization yields an asymmetric η^2-O,O coordination mode:[16]

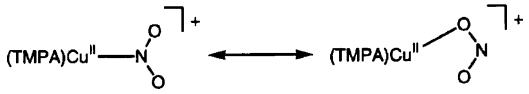

N-coordinated nitrite to copper(II) is very rare, and the potential differences in electronic structure between the N- and O-bound isomers have not been analyzed yet.

So far, the detailed evaluation of second coordination sphere effects on the properties of copper nitrite and nitric oxide complexes were mostly limited on Cu(I)−nitrosyls and

(4) (a) Godden, J. W.; Turley, S.; Teller, D. C.; Adman, E. T.; Liu, M. Y.; Payne, W. J.; LeGall, J. *Science* **1991**, *253*, 438. (b) Adaman, E. T.; Godden, J. W.; Turley, S. *J. Biol. Chem.* **1995**, *270*, 27458. (c) Murphy, M. E. P.; Turley, S.; Kukimoto, M.; Nishiyama, M.; Horinouchi, S.; Sasaki, H.; Tanokura, M.; Adman, E. T. *Biochemistry* **1995**, *34*, 12107. (d) Murphy, M. E. P.; Turley, S.; Adman, E. T. *J. Biol. Chem.* **1997**, *45*, 28455. (e) Dodd, F. E.; Van Beeumen, J.; Eady, R. R.; Hasnain, S. S. *J. Mol. Biol.* **1998**, *282*, 369. (f) Inoue, T.; Gotowda, M.; Deligeer Kataoka, M.; Yamaguchi, K.; Suzuki, S.; Watanabe, H.; Gohow, M.; Kai, Y. *J. Biochem.* **1998**, *124*, 876.
(5) Libby, E.; Averill, B. A. *Biochim. Biophys. Res. Commun.* **1992**, *187*, 1529.
(6) (a) Strange, R. W.; Dodd, F. E.; Abraham, Z. H. L.; Grossmann, J. G.; Brüser, T.; Eady, R. R.; Smith, B. E.; Hasnain, S. S. *Nat. Struct. Biol.* **1995**, *2*, 287. (b) Howes, B. D.; Abraham, Z. H. L.; Lowe, D. J.; Brüser, T.; Eady, R. R.; Smith, D. E. *Biochemistry* **1994**, *33*, 3171.
(7) Tocheva, E. I.; Rosell, F. I.; Mauk, A. G.; Murphy, M. E. P. *Science* **2004**, *304*, 867−870.
(8) Kataoka, K.; Furusawa, H.; Takagi, K.; Yamaguchi, K.; Suzuki, S. *J. Biochem.* **2000**, *127*, 345.
(9) (a) Veselov, A.; Olesen, K.; Sienkiewicz, A.; Shapleigh, J. P.; Scholes, C. P. *Biochemistry* **1998**, *37*, 6095. (b) Olesen, K.; Veselov, A.; Zhao, Y.; Wang, Y.; Danner, B.; Scholes, C. P.; Shapleigh, J. P. *Biochemistry* **1998**, *37*, 6086. (c) Strange, R. W.; Murphy, L. M.; Dodd, F. E.; Abraham, Z. H. L.; Eady, R. R.; Smith, B. E.; Hasnain, S. S. *J. Mol. Biol.* **1999**, *287*, 1001.
(10) Prudêncio, M.; Eady, R. R.; Sawers, G. *Biochem. J.* **2001**, *353*, 259.
(11) (a) Halfen, J. A.; Mahapatra, S.; Olmstead, M. M.; Tolman, W. B. *J. Am. Chem. Soc.* **1994**, *116*, 2173. (b) Halfen, J. A.; Tolman, W. B. *J. Am. Chem. Soc.* **1994**, *116*, 5475. (c) Halfen, J. A.; Mahapatra, S.; Wilkinson, E. C.; Gengenbach, A. J.; Young, V. G., Jr.; Que, L., Jr.; Tolman, W. B. *J. Am. Chem. Soc.* **1996**, *118*, 763. (d) Kujime, M.; Fujii, H. *Angew. Chem.* **2006**, *118*, 1107.
(12) Yokoyama, H.; Yamaguchi, K.; Sugimoto, M.; Suzuki, S. *Eur. J. Inorg. Chem.* **2005**, 1435.
(13) Antonyuk, S. V.; Strang, R. W.; Sawers, G.; Eady, R. R.; Hasnain, S. S. *Proc. Natl. Acad. Sci. U.S.A.* **2005**, *102*, 12041.
(14) Schneider, J. L.; Carrier, S. M.; Ruggiero, C. E.; Young, V. G., Jr.; Tolman, W. B. *J. Am. Chem. Soc.* **1998**, *120*, 11408−11418.
(15) Tolman, W. B. *Inorg. Chem.* **1991**, *30*, 4877−4880.
(16) Komeda, N.; Nagao, H.; Kushi, Y.; Adachi, G.; Suzuki, M.; Uehara, A.; Tanaka, K. *Bull. Chem. Soc. Jpn.* **1995**, *68*, 581.

anionic hydrotris(pyrazolyl)borate ligands.[14,17] In this paper, tripodal substituted tris(pyrazolyl)methane (L′) and hydrotris(pyrazolyl)borate (L^-), and dipodal bis(pyrazolyl)methane (L″) ligands are applied to investigate the effect of (a) the total charge of the ligands (neutral in L′ and anionic in L^-), (b) the coordination number of the ligands (three in L′ and two in L″), and (c) the nature of the pyrazolyl substituents, on the structures and spectroscopic properties of Cu(II)−nitrito complexes. Crystal structures for nitrito complexes with each type of ligand are presented. The electronic structures of the compounds are investigated using vibrational (IR and resonance Raman) and electronic (UV−vis absorption and magnetic circular dichroism (MCD)) spectroscopies coupled to DFT calculations. This way, second coordination sphere effects in this class of compounds are analyzed in detail.

Experimental and Computational Procedures

General Materials. Preparation and handling of all complexes were performed under an argon atmosphere by employing standard Schlenk line techniques or a glovebox. Dichloromethane and acetonitorile were distilled from P_2O_5 and CaH_2 prior to use, respectively. Diethyl ether and heptane were carefully purified by refluxing/distilling under an argon atmosphere over sodium benzophenone ketyl.[18] Ethanol, methanol, and acetone were spectroscopic grade and were used after bubbling with argon gas. $Na^{15}NO_2$ was purchased from Cambridge Isotope Laboratories, Inc. Other reagents were used without further purification unless otherwise noted. KL1 ($L1^- = HB(3,5\text{-}i\text{-}Pr_2pz)_3^-$),[19] KL3 ($L3^- = HB(3\text{-}t\text{-}Bu,5\text{-}i\text{-}Prpz)_3^-$),[20] L1′ ($L1' = HC(3,5\text{-}i\text{-}Pr_2pz)_3$),[21] and [Cu(L3)-$(NO_3)$],[22] and [Cu(L1′)$(NO_3)_2$][21a] were prepared as previously reported.

Syntheses. $H_2C(3,5\text{-}i\text{-}Pr_2pz)_2$ (L1″). The ligand L1″ was synthesized by a modified method from ref 23. Dichloromethane (130 cm^3) was added to a mixture of 3,5-diisopropylpyrazole[19] (9.03 g, 40 mmol), potassium carbonate (35.0 g), and tetrabutylammonium hydrogensulfate (2.50 g), and the solution was bubbled with argon gas for 15 min. This solution was then heated and gently refluxed for 7 days in an autoclave (the inner temperature ∼115 °C). During the reaction the color of the solution turned dark brown. The solution was allowed to cool to room temperature, and the insoluble material was filtered and washed with acetone. The solution was dried in vacuo. The remaining brown oil was dissolved in a 1:2 mixture of diethyl ether/hexane (30 cm^3). This solution was chromatographed on a silica gel column using the 1:2 ether/hexane mixed solvent as eluent. After collection of the corresponding fractions, the solvent was removed under vacuum to yield a white powder. Recrystallization from acetonitrile at −30 °C gave colorless crystals (6.63 g, 20.9 mmol, 71% yield). ^{1}H NMR (600 MHz, $CDCl_3$): δ (ppm) 6.22 (s, 2H, *H*C), 5.85 (s, 2H, 4-*H*(pz)), 3.40 (sept, J_{HH}= 6.9 Hz, 2H, C*H*$(CH_3)_2$), 2.90 (sept, J_{HH}= 6.9 Hz, 2H, C*H*$(CH_3)_2$), 1.22 (d, J_{HH}= 6.8 Hz, 12H, CH(C*H*$_3)_2$), 1.04 (d, J_{HH}= 6.8 Hz, 12H, CH(C*H*$_3)_2$). ^{13}C NMR (150 MHz, $CDCl_3$): δ (ppm) 158.3 (5-*C* (pz)), 151.5 (3-*C* (pz)), 99.7 (4-*C* (pz)), 62.1 (H_2C), 27.8 (*C*H$(CH_3)_2$), 24.9 (*C*H$(CH_3)_2$), 23.1 (CH(*C*H$_3)_2$), 22.8 (CH-(*C*H$_3)_2$). FT-IR (KBr, cm^{-1}): 1549 ν(CN). Anal. Calcd for $C_{19}H_{32}N_4$: C, 72.11; H, 10.19; N, 17.70. Found: C, C, 72.11; H, 9.80; N, 17.74.

[Cu(L1)(η^2-ONO)] (1). To a solution of [Cu(L1)Cl][24] (0.502 g, 0.888 mmol) in dichloromethane (20 cm^3) was added $NaNO_2$ (0.0685 g, 0.993 mmol) dissolved in methanol (10 cm^3) . The color of the solution gradually turned to green, and a small amount of white solid precipitated. After having been stirred for 1 h, the solvent was removed under vacuum. The residue was extracted with dichloromethane, and undissolved powder was filtered off using Celite. The filtrate was evaporated under reduced pressure to give a green solid. Recrystallization from acetonitrile at −30 °C gave green crystals (0.245 g, 48%). Single crystals suitable for X-ray diffraction were obtained by slow recrystallization from dichloromethane/ether at −30 °C. EPR (dichloromethane/1,2-dichloroethane, 140 K) $g_{//}$ 2.32, $A_{//}$ 129 G, $g_\perp$ 2.10. Anal. Calcd for $C_{27}H_{46}N_7BCuO_2$: C, 56.39; H, 8.06; N, 17.05. Found: C, 56.57; H, 8.33; N, 16.95.

[Cu(L3)(η^2-ONO)] (2). The preparation of **2** was carried out by the same method as that for **1** using [Cu(L3)Cl][25] (0.267 g, 0.439 mmol) and $NaNO_2$ (0.0350 g, 0.507 mmol). Recrystallization from dichloromethane/ether at −30 °C gave brown crystals (0.182 g, 67%). Single crystals suitable for X-ray diffraction were obtained by slow recrystallization from a dichloromethane/ether solution at room temperature. EPR (dichloromethane/1,2-dichloroethane, 140 K) $g_\perp$ 2.18, $g_{//}$ 2.03, $A_{//}$ 116 G. Anal. Calcd for $C_{30}H_{52}N_7BCuO_2$: C, 58.39; H, 8.49; N, 15.89. Found: C, 57.78; H, 8.35; N, 15.71.

[Cu(L1)($^{15}NO_2$)] and [Cu(L3)($^{15}NO_2$)]. Each ^{15}N labeled complex was prepared by the same method as the corresponding unlabeled complex using $Na^{15}NO_2$.

[Cu(L1′)(η^1-ONO)(η^1-NO_2)] (3). The preparation of **3** was carried out by the same method as that for **1** using [Cu(L1′)Cl_2][21a] (0.158 g, 0.263 mmol) and $NaNO_2$ (0.0425 g, 0.616 mmol). Recrystallization from chloroform at −30 °C gave green crystals (0.245 g, 48%). EPR (dichloromethane/1,2-dichloroethane, 140 K) $g_{//}$ 2.31, $A_{//}$ 146 G, $g_\perp$ 2.10. Anal. Calcd for $C_{28}H_{46}N_8CuO_4$: C, 51.40; H, 7.09; N, 17.13. Found: C, 51.38; H, 7.15; N, 17.09.

[Cu(L1″)(η^1-ONO)$_2$] (4). To a solution of [Cu(L1″)Cl_2][26] (0.253 g, 0.577 mmol) in dichloromethane (25 cm^3) was added $NaNO_2$ (0.082 g, 1.19 mmol) dissolved in methanol (15 cm^3) . The color of the solution gradually turned to deep green. After having been stirred for 1 h, the solvent was removed under vacuum. The residue was extracted with dichloromethane, and undissolved powder was filtered off using Celite. The solution was then concentrated by removal of solvent under reduced pressure. Recrystallization from dichloromethane/heptane at −30 °C gave deep green crystals (0.201 g, 74% yield). Single crystals suitable for X-ray diffraction were

(17) Ruggiero, C. E.; Carrier, S. M.; Antholine, W. E.; Whittaker, J. W.; Cramer, C. J.; Tolman, W. B. *J. Am. Chem. Soc.* **1993**, *115*, 11285.
(18) Armarego, W. L. F.; Perrin, D. D. *Purification of Laboratory Chemicals*, 4th ed.; Butterworth-Heinemann: Oxford, 1997.
(19) Kitajima, N.; Fujisawa, K.; Fujimoto, C.; Moro-oka, Y.; Hashimoto, S.; Kitagawa, T.; Toriumi, K.; Tatsumi, K.; Nakamura, A. *J. Am. Chem. Soc*. **1992**, *114*, 1277.
(20) Imai, S.; Fujisawa, K.; Kobayashi, T.; Shirasawa, N.; Fujii, H.; Yoshimura, T.; Kitajima, N.; Moro-oka, Y. *Inorg. Chem.* **1998**, *37*, 3066−3070.
(21) (a) Fujisawa, K.; Ono, T.; Aoki, H.; Ishikawa, Y.; Miyashita, Y.; Okamoto, K.; Nakazawa, H.; Higashimura, H. *Inorg. Chem. Commun.* **2004**, *7*, 330−332. (b) Fujisawa, K.; Ono, T.; Ishikawa, Y.; Amir, N.; Miyashita, Y.; Okamoto, K.; Lehnert, N. *Inorg. Chem.* **2006**, *45*, 1698−1713.
(22) Fujisawa, K.; Kobayashi, T.; Fujita, K.; Kitajima, N.; Moro-oka, Y.; Miyashita, Y.; Yamada, Y.; Okamoto, K. *Bull. Chem. Soc. Jpn.* **2000**, *73*, 1797−1804.
(23) Tang, L.-F.; Zhao, S.-B.; Jia, W.-L.; Yang, Z.; Song, D.-T.; Wang, J.-T. *Organometallics* **2003**, *22*, 3290.
(24) Kitajima, N.; Fujisawa, K.; Moro-oka, Y. *J. Am. Chem. Soc.* **1990**, *112*, 3210−3212.
(25) Fujisawa, K.; Tada, N.; Ishikawa, Y.; Higashimura, H.; Miyashita, Y.; Okamoto, K. *Inorg. Chem. Commun*. **2004**, *7*, 209−212.
(26) Fujisawa, K. Manuscript in preparation.

Table 1. Summary of Crystallographic Data of **1**, **2**, **4**, and **5**

complex	**1**	**2**	**4**·(CH_2Cl_2)	**5**
color, habit	green, prism	red, prism	green, block	blue, block
formula	$C_{27}H_{46}N_7BCuO_2$	$C_{30}H_{52}N_7BCuO_2$	$C_{20}H_{34}N_6CuO_4Cl_2$	$C_{19}H_{32}N_6CuO_6$
formula weight	575.06	617.14	556.98	504.04
crystal system	monoclinic	monoclinic	triclinic	triclinic
space group	*P*21/*c* (#14)	*P*21/*c* (#14)	$P\bar{1}$ (#2)	$P\bar{1}$ (#2)
a, Å	10.008(4)	9.494(3)	8.2462(5)	9.017(3)
b, Å	19.188(7)	17.488(5)	9.7908(5)	10.374(4)
c, Å	16.541(7)	20.792(6)	18.3590(9)	13.917(5)
α, deg			90.679(2)	81.215(9)
β , deg	106. 065(5)	107.125(3)	98.948(2)	72.996(6)
γ, deg			114.061(2)	84.007(10)
V, Å^3	3052.2(20)	3298.9(17)	1332.32(12)	1227.8(7)
Z	4	4	2	2
D_{calc}, g/cm^3	1.251	1.242	1.388	1.363
μ(Mo Kα), cm^{-1}	7.51	6.99	10.56	9.34
temp, °C	−66	−66	−90	−69
2θ range, deg	6−55	6−55	6−55	6−55
reflections collected	24591	25984	11046	9856
unique reflections	6929	7471	10900	5503
R_{int}	0.043	0.032	0.018	0.023
no. of observations	5009 ($I > 3\sigma(I)$)	5704 ($I > 3\sigma(I)$)	9921($I > 5\sigma(I)$)	4766($I > 3\sigma(I)$)
no. of variables	389	422	332	321
R^a	0.070	0.046	0.061	0.038
$R_w{}^a$	0.069	0.042	0.094	0.038
good. of fit ind.	2.78	2.38	4.96	2.26
max/min peak, e/Å^3	0.86/−0.67	0.42/−0.38	4.63/−3.43	0.39/−0.37

[a] $R = \sum||F_o| - |F_c||/\sum|F_o|$; $R_w = [(\sum w(|F_o| - |F_c|)^2/\sum wF_o^2)]^{1/2}$, $w = 1/\sigma^2(|F_o|)$.

obtained by slow recrystallization under the same experimental conditions. EPR (methanol, 140 K) $g_{//}$, 2.31, $A_{//}$, 153 G; $g_\perp$, 2.07. Anal. Calcd for $C_{19}H_{32}N_6CuO_4$·0.15CH_2Cl_2: C, 47.42; H, 6.71; N, 17.32. Found: C, 47.53; H, 6.65; N, 17.13.

[Cu(L1″)(η^1-NO_3)$_2$] (5). To a solution of $Cu(NO_3)_2$·3H_2O (0.174 g, 0.722 mmol) in acetone (20 cm^3) was added L1″ (0.203 g, 0.643 mmol) dissolved in dichloromethane (20 cm^3). The color of the solution gradually turned deep blue. After having been stirred for 1 h, the solvent was removed under vacuum. The residue was extracted with dichloromethane, and undissolved powder was filtered off using Celite. The solution was then concentrated by removal of solvent under reduced pressure. Recrystallization from dichloromethane/heptane at −30 °C gave blue crystals (0.275 g, 85% yield). Single crystals suitable for X-ray diffraction were obtained by slow recrystallization under the same experimental conditions. EPR (methanol, 140 K) $g_{//}$, 2.33, $A_{//}$, 147 G, $g_\perp$, 2.07. Anal. Calcd for $C_{19}H_{32}N_6CuO_6$: C, 45.28; H, 6.40; N, 16.67. Found: C, 45.10; H, 6.07; N, 16.55.

Crystal Structure Determination. Crystal data and refinement parameters for **1**, **2**, **4**, and **5** are given in Table 1. The diffraction data were measured on a Rigaku/MSC Mercury CCD system with graphite monochromated Mo Kα ($\lambda = 0.71069$ Å) radiation at low temperature. All crystals were mounted on glass fiber using epoxy glue. The unit cell parameters of each crystal were obtained using Rigaku Daemon software and refined using CrystalClear on all observed reflections.[27] Data using 0.5° intervals in ϕ and ω for 35 s/frame (**1**), for 30 s/frame (**2**), for 30 s/frame (**4**), and for 40 s/frame (**5**) were collected with a maximum resolution of 0.77 Å (744 oscillation images). The highly redundant data sets were reduced using CrystalClear and corrected for Lorentz and polarization effects. An empirical absorption correction was applied for each complex.[28] Structures were solved by direct methods using the program SIR 92.[29] The position of the metal atoms and their first coordination sphere were located from a direct method *E*-map; other non-hydrogen atoms were found in alternating difference Fourier syntheses[30] and least-squares refinement cycles. These were refined anisotropically during the final cycles (CrystalStructure).[28] Hydrogen atoms were placed in calculated positions. The structure of **3** has not been completed because of the poor quality of the crystals obtained (usually very small) and the presence of highly disordered molecules (both nitrite and solvent). The GOF value of **4** is of lower quality due to a disordered dichloromethane molecule. Crystallographic data and structure refinement parameters including the final discrepancies (R and R_w) are listed in Table 1.

UV−vis Spectroscopy. Solid-state absorption spectra have been recorded either on KBr disks or for pure solids (between sapphire windows) at 10 K using a Varian Cary 5 UV−vis-NIR spectrometer equipped with a CTI cryocooler. Solution spectra in the 260−1400 nm range were measured with a JASCO V-570 spectrophotometer at room temperature using a quartz cell (1.0 cm path length).

Vibrational Spectroscopy. Resonance Raman spectra were measured on a Dilor XY Raman spectrograph with triple monochromator and CCD detector. An Ar/Kr mixed-gas laser with a maximum power of 5 W was used for excitation. Spectra were recorded at excitation wavelengths of 454.5, 488.0, 514.5, 568.2, and 647.1 nm. The spectra were measured on KBr disks cooled to 10 K with a helium cryostat. The spectral bandpass was set to 2 cm^{-1}. Middle- and far-infrared spectra (MIR and FIR) were recorded on a Bruker IFS 66v vacuum instrument and a JASCO FT/IR-550 spectrophotometer at room temperature. For the MIR region, KBr disks were used, and the spectra were recorded at a

(27) CrystalClear Ver. 1.3: Pflugrath, J. W. *Acta Crystallogr.* **1999**, *D55*, 1718.

(28) (a) *CrystalStructure 3.70: Crystal Structure Analysis Package*; Rigaku and Rigaku/MSC, 2005. (b) Watkin, D. J.; Prout, C. K.; Carruthers, J. R.; Betteridge, P. W. *Crystal Issue 10*; Chemical Crystallography Laboratory: Oxford, U.K., 1996.

(29) SIR92: Altomare, A.; Cascarano, G.; Giacovazzo, C.; Guagliardi, A.; Burla, M.; Polidori, G.; Camalli, M. *J. Appl. Crystallogr.* **1994**, *27*, 435.

(30) DIRDIF-99: Beurskens, P. T.; Admiraal, G.; Beurskens, G.; Bosman, W. P.; de Gelder, R.; Israel, R.; Smits, J. M. M. *The DIRDIF-99 program system*; Technical Report of the Crystallography Laboratory; University of Nijmegen: The Netherlands, 1999.

resolution of 1 cm^{-1}. In the FIR region, PE pellets were used, and the resolution was set to 2 cm^{-1}.

MCD Spectroscopy. Magnetic circular dichroism spectra were obtained on a setup consisting of a JASCO J-715 spectropolarimeter and an Oxford Instruments SPECTROMAG magnetocryostat which is capable of generating magnetic fields up to 11T. Spectra were taken in mulls in order to ensure that the spectra obtained can be directly related to the crystal structures of the compounds.

Other Instruments. EPR spectra were recorded on a Bruker EMX-T EPR spectrometer in frozen solution (dichloromethane/1,2-dichloroethane (1:1) or methanol) at low temperature in quartz tubes (diameter 5 mm) with liquid-nitrogen temperature controller BVT 3000. ^{1}H NMR (600 MHz) and ^{13}C NMR (150 MHz) spectra were recorded on a Bruker AVANCE-600 at ambient temperature in $CDCl_3$. Chemical shifts were reported as δ values downfield from the internal standard $(CH_3)_4Si$. Elemental analysis (C, H, N) was performed by the Chemical Analysis Center of the University of Tsukuba.

Density Functional Calculations. DFT calculations for the tris(pyrazolyl)borate complexes **1** and **2** were performed using the simplified model [Cu(tPB)(NO_2)] (**1a**−**1f**) in order to explore the flexibility of the coordination geometry of nitrite. In this model, the ligand hydrotris(pyrazolyl)borate (tPB) with truncated side chains was applied. Using this model, three different coordination modes of nitrite could be obtained in one system which allows for a direct comparison of the absolute energies of these species. In the case of the complexes **3** and **4** where two nitrite ions are bound to copper, geometry optimizations were performed on model systems that include the isopropyl side chains of the tris/bis(pyrazolyl)methane ligands that face the nitrite binding site. This way, any kind of steric interactions between the nitrite ions and the ligand side chains is incorporated in the resulting model systems $\tilde{\mathbf{3}}$ and $\tilde{\mathbf{4}}$, respectively. The geometries of all model systems were optimized using BP86/TZVP. Vibrational frequencies were also calculated with this method. Single point energies on the different isomers of [Cu(tPB)(NO_2)] were obtained from B3LYP calculations applying a mixed basis set: TZV(2p1f) for Cu, TZV(2d) for the ligand, and TZV(p) for H. TD-DFT calculations were performed using the Tamm-Dancoff approximation. All calculations on the [Cu(tPB)(NO_2)] models and the TD-DFT calculations were performed with the program ORCA.[31] Calculations on models $\tilde{\mathbf{3}}$ and $\tilde{\mathbf{4}}$ were performed using Gaussian 03.[32]

Results and Analysis

A. Copper(II)−Nitrito Complexes with Hydrotris(pyrazolyl)borate Coligands (1 and 2). A.1. Crystal Structure.

The reaction of copper(II) chloro complexes with $NaNO_2$ in the mixed dichloromethane/methanol solvent at room temperature readily gives the corresponding copper(II)−nitrito complexes [Cu(L1)(ONO)] (**1**) and [Cu(L3)(ONO)] (**2**) in high yield as shown in eq 1 for **1**. Selected bond distances and angles for all complexes are given in Table 2. Since both complexes are neutral, the oxidation state of the copper ions is +II in both cases.

Table 2. Selected Bond Distances (Å) and Angles (deg) for **1**, **2**, **4**, and **5**

	1	**2**	**4**	**5**
		Bond Distances		
Cu1−N11	1.966(3)	2.063(2)	1.970(2)	1.968(2)
Cu1−N21	2.110(3)	2.091(2)	2.039(2)	2.010(1)
Cu1−N31	1.996(2)	1.9651(15)		
Cu1−O31			1.984(2)	1.970(2)
Cu1−O41	2.022(3)	1.9872(15)	2.024(2)	2.014(1)
Cu1−O42	2.031(3)	2.195(2)	2.370(3)	
		Bond Angles		
N11−Cu1−N21	90.84(14)	100.94(8)	89.28(8)	90.04(6)
N11−Cu1−N31	91.38(12)	90.62(7)		
N21−Cu1−N31	91.91(12)	90.80(7)		
N11−Cu1−O31			172.0(1)	172.38(7)
N21−Cu1−O31			95.42(8)	95.36(6)
N11−Cu1−O41	102.79(15)	95.93(7)	90.44(8)	89.32(6)
N21−Cu1−O41	113.10(16)	95.95(7)	162.9(1)	164.24(7)
N31−Cu1−O41	150.68(18)	169.53(8)		
N11−Cu1−O42	160.60(15)	129.18(8)	94.47(8)	
N21−Cu1−O42	103.64(15)	122.85(8)	106.27(9)	
N31−Cu1−O42	100.83(14)	111.35(8)		
O41−Cu1−O42	59.80(16)	58.21(8)	56.70(9)	
O31−Cu1−O41			86.98(8)	86.95(6)
O31−Cu1−O42			90.48(9)	

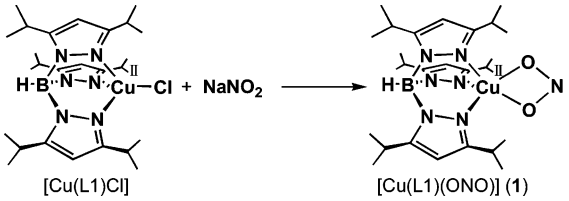

(1)

The obtained structures are in general similar to those obtained for other Cu(II)−nitrito complexes with different hydrotris(pyrazolyl)borate ligands.[15,33] Complex [Cu(L1)(η^2-ONO)] (**1**) crystallizes in the monoclinic space group $P2_1/c$ and has a mononuclear structure as shown in Figure 1. Using the geometry descriptor τ introduced by Addison et al.,[34] the coordination geometry of **1** yields a value of $\tau = 0.17$. This means that **1** has a slightly distorted square pyramidal geometry. The deviation of the copper(II) ion from the corresponding N_2O_2 plane in the apical direction is 0.30(1) Å. As expected, the Cu−N distance at the apical position is slightly longer than those in the basal plane. The nitrite ligand in **1** is in a symmetric bidentate coordination mode (Cu1−O41 = 2.022(4) Å and Cu1−O42 = 2.031(4) Å; ΔCu−O

(31) Neese, F. *ORCA, version 2.2*; Max-Planck Institut für Bioanorganische Chemie: Mülheim/Ruhr, Germany, 2004.
(32) Frisch, M. J.; Trucks, G. W.; Schlegel, H. B.; Scuseria, G. E.; Robb, M. A.; Cheeseman, J. R.; Montgomery, J. A., Jr.; Vreven, T.; Kudin, K. N.; Burant, J. C.; Millam, J. M.; Iyengar, S. S.; Tomasi, J.; Barone, V.; Mennucci, B.; Cossi, M.; Scalmani, G.; Rega, N.; Petersson, G. A.; Nakatsuji, H.; Hada, M.; Ehara, M.; Toyota, K.; Fukuda, R.; Hasegawa, J.; Ishida, M.; Nakajima, T.; Honda, Y.; Kitao, O.; Nakai, H.; Klene, M.; Li, X.; Knox, J. E.; Hratchian, H. P.; Cross, J. B.; Adamo, C.; Jaramillo, J.; Gomperts, R.; Stratmann, R. E.; Yazyev, O.; Austin, A. J.; Cammi, R.; Pomelli, C.; Ochterski, J. W.; Ayala, P. Y.; Morokuma, K.; Voth, G. A.; Salvador, P.; Dannenberg, J. J.; Zakrzewski, V. G.; Dapprich, S.; Daniels, A. D.; Strain, M. C.; Farkas, O.; Malick, D. K.; Rabuck, A. D.; Raghavachari, K.; Foresman, J. B.; Ortiz, J. V.; Cui, Q.; Baboul, A. G.; Clifford, S.; Cioslowski, J.; Stefanov, B. B.; Liu, G.; Liashenko, A.; Piskorz, P.; Komaromi, I.; Martin, R. L.; Fox, D. J.; Keith, T.; Al-Laham, M. A.; Peng, C. Y.; Nanayakkara, A.; Challacombe, M.; Gill, P. M. W.; Johnson, B.; Chen, W.; Wong, M. W.; Gonzalez, C.; Pople, J. A. Gaussian, Inc.: Pittsburgh, PA, 2003.
(33) Ruggiero, C. E.; Carrier, S. M.; Tolman, W. B. *Angew. Chem., Int. Ed. Engl.* **1994**, *33*, 895.
(34) This coordination geometry is supported by the structural parameter τ; $\tau = (\alpha - \beta)/60°$, where α and β are the largest angles ($\alpha > \beta$) around a five-coordinate metal center. The parameter τ is equal to 0 for an ideal square-planar geometry, while for a perfect trigonal-bipyramidal geometry it becomes 1. Addison, A. W.; Rao, T. N.; Reedijk, J.; van Rijn, J.; Verschoor, G. C. *J. Chem. Soc., Dalton Trans.* **1984**, 1349.

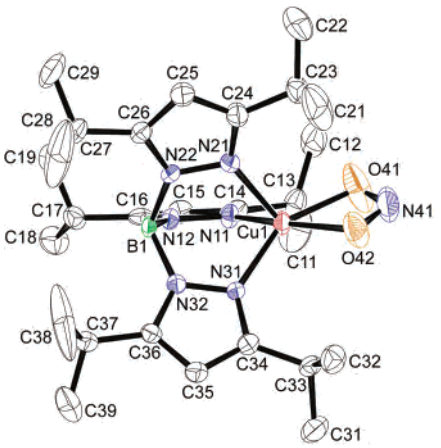

Figure 1. Crystal structure of [Cu(L1)(η^2-ONO] (**1**) (50% probability ellipsoids shown).

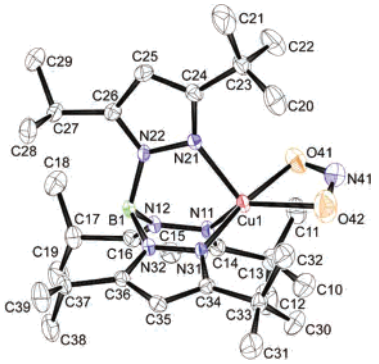

Figure 2. Crystal structure of [Cu(L3)(η^2-ONO] (**2**) (50% probability ellipsoids shown).

= 0.009(4) Å). Compound [Cu(L3)(η^2-ONO)] (**2**) crystallizes in the form of well separated molecules in the $P2_1/c$ space group. The τ value[34] in **2** is 0.67, which corresponds to a highly distorted trigonal bipyramidal geometry with the basal plane consisting of two nitrogen atoms (N11 and N21) from hydrotris(pyrazolyl)borate and one oxygen atom (O42) from NO_2^-as shown in Figure 2. Further, the Cu−N31 distance at the apical position is much shorter than those in the basal plane. Correspondingly, the Cu−O42 distance at the apical position is shorter by 0.208(2) Å than Cu−O41. This indicates that the interaction between the copper(II) ion and the apical ligands is distinctively stronger compared to the interaction with the ligands in the basal plane, which is indicative of a d_{z^2} ground state in **2**. This is also evident from EPR ($g_\perp = 2.18$, $g_{//} = 2.03$, $A_{//} = 116$ G). The nitrite ligand in **2** shows an asymmetric bidentate coordination mode due to the trigonal bipyramidal coordination geometry described above.

Comparing the known crystal structures for copper(II)−nitrito complexes ligated by hydrotris(pyrazolyl)borate, the nitrite binding mode shifts from symmetric bidentate (ΔCu−O = 0 Å) in [Cu{HB(3,5-Me_2pz)$_3$}(ONO)][33] and ΔCu−O = 0.009(4) Å in **1** to essentially asymmetric bidentate (ΔCu−O = 0.193(6) Å) in [Cu{HB(3-tBupz)$_3$(ONO)}][15] and ΔCu−O = 0.208(2) Å in **2**. These differences in the nitrite binding geometry can be viewed as a direct reflection of the divergent steric influences of the alkyl substituted hydrotris(pyrazolyl)-borate ligands.[33] This interpretation is further substantiated by the corresponding nitrato complexes:[22,35] [Cu(L1)(η^2-NO_3)] and [Cu(L3)(η^2-NO_3)] show the same geometrical changes going from a slightly distorted square pyramidal (τ = 0.22, ΔCu−O (nitrate) = 0.044(3) Å in [Cu(L1)(NO_3)]) to a highly distorted trigonal bipyramidal geometry (τ = 0.77, ΔCu−O (nitrate) = 0.217(3) Å in [Cu(L3)(NO_3)]).

A.2. Vibrational Spectra and Assignment. The IR spectrum of [Cu(L1)(η^2-ONO)] (**1**) is shown in Figure 3 together with the corresponding ^{15}N isotope labeled data. The identification of the vibrations of the Cu−NO_2^- subunit is complicated by the fact that the spectra are dominated by intense bands of the hydrotris(pyrazolyl)borate ligand. Table 3 summarizes the assignments. The band at 1287 cm^{-1} shifts to 1263 cm^{-1} on ^{15}N substitution. In agreement with the calculations (cf. Table 3), this feature is assigned to the symmetric N−O stretch ν_s(N−O) of nitrite. At lower energy, the corresponding antisymmetric stretch ν_{as}(N−O) is identified with the band at 1197 cm^{-1} that disappears in the ^{15}N labeled compound. It probably shifts into the intense band at ∼1175 cm^{-1} and is masked by this feature. This sequence with ν_s(N−O) at higher energy than ν_{as}(N−O) is also found in "free" nitrite like $LiNO_2$, etc., but is in contrast to the assignments for six-coordinate nitrito complexes in the literature[16] (see Discussion). In addition, this is also in contrast to previous assignments of the N−O stretching modes for a related Cu(II)−NO_2^- complex with a substituted hydrotris(pyrazolyl)borate coligand.[14,15] At 877 cm^{-1}, the O−N−O bending mode of nitrite is found in the IR spectrum of complex **1**. This band shows a small ^{15}N isotope shift to 872 cm^{-1}. Finally, the isotope sensitive band at 358 cm^{-1} is assigned to the Cu−O stretch. Since nitrite binds to Cu(II) with both its oxygens, it is not clear whether this band belongs to the corresponding symmetric or antisymmetric vibration. From the calculations, ν_s(Cu−O) is predicted around 360 cm^{-1} (cf. Table 3) and at distinctively higher energy than ν_{as}(Cu−O). Therefore, the band at 358 cm^{-1} is assigned to ν_s(Cu−O). Another interesting feature in the IR spectrum of **1** is found at 2551 cm^{-1} which belongs to the B−H stretch of the hydrotris(pyrazolyl)borate ligand. The Raman spectra of **1** are shown in Figure S3. Only the symmetric N−O stretch is found in these data at 1284 cm^{-1} shifting to 1262 cm^{-1} on isotope substitution in accordance with the IR results. The fact that this mode appears in the Raman spectra is in agreement with its assignment to the symmetric N−O stretch, which should be Raman active.

The Supporting Information (Figures S4 and S5) also contains the IR and Raman spectra of [Cu(L3)(η^2-ONO)] (**2**) and of the corresponding $^{15}NO_2^-$ complex. In this case, the spectroscopic information is less complete. In particular, the Raman spectra of **2** do not show the intense ν_s(N−O) feature as in the case of **1**, which might be due to the asymmetric binding mode of nitrite in this complex. As shown in Table 3, the observed vibrational energies for **2** are close to the ones observed for **1** further supporting the assignments described above. Hence, the difference in binding mode between **1** and **2** does not seem to have much

(35) Fujisawa, K.; Miyashita, Y.; Yamada, Y.; Okamoto, K. *Bull. Chem. Soc. Jpn.* **2001**, *74*, 1065−1066.

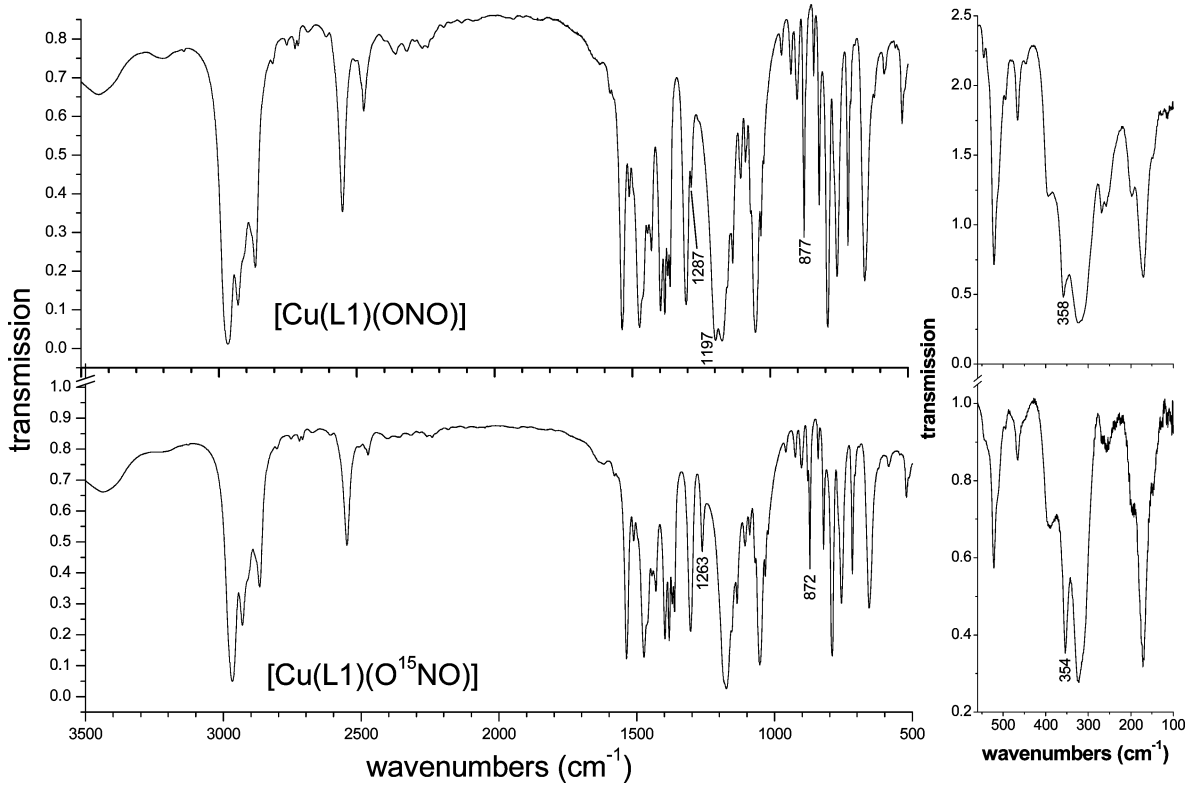

Figure 3. IR spectrum of **1** (top) and of the corresponding $^{15}NO_2^-$ isotope labeled complex (bottom).

Table 3. Comparison of Experimental and Calculated Vibrational Frequencies of Cu(II)−NO_2^- Complexes

		vibration				
compound[a]		ν_s(N−O)	ν_{as}(N−O)	δ(O−N−O)	ν_s(Cu−O)	ν_{as}(Cu−O)
[Cu(L1)(η^2-ONO] (**1**)	IR	1287	1197	877	358	
	R	1284				
[Cu(L1)(η^2-O^{15}NO]	IR	1263	*b*	872	354	
	R	1262				
[Cu(L3)(η^2-ONO] (**2**)	IR	1264	*b*	875	*b*	
	R		1182			
[Cu(L3)(η^2-O^{15}NO]	IR	*b*	1162	870	*b*	
	R		∼1160			
[Cu(tPB)(η^2-ONO)] − calc		1248	1098	833	360/316	313
[Cu(tPB)(η^1-ONO)] − calc		1249	1097	833	360/316	312
[Cu(tPB)(η^1-NO_2)] − calc		1231	1461	772	381/296[c]	

[a] 'tPB' = hydrotris(pyrazolyl)borate; this is the simplified ligand used for the calculations (see Experimental Section). [b] This band is most probably masked by other intense features. [c] Here: ν(Cu−N).

effect on the vibrational energies in agreement with the calculations (Table 3).

A.3. Electronic Spectra. Figure 4 shows the UV−vis absorption and MCD spectra of [Cu(L1)(η^2-ONO)]. The corresponding data of [Cu(L3)(η^2-ONO)] and [Cu(L3)(η^2-NO_3)] are presented in Figures S7 and S8, respectively. As one can see from these plots, the two Cu(II)−NO_2^- spectra are comparable in appearance to the Cu(II)−NO_3^- data. Hence, Cu(II)−nitrite LMCT transitions are not readily discernible below 40 000 cm^{-1}. In addition, the spectra of **1** with the $L1^-$ ligand have the same overall appearance as the spectra of **2** with ligand $L3^-$. This is somewhat surprising considering the different ground states of these complexes as determined from EPR (vide supra). Hence, the MCD results indicate that the influence of the different ground states on the electronic spectra is limited. Table 4 lists the band positions obtained from simultaneous Gaussian fits of the absorption and MCD spectra of **1**, **2**, and [Cu(L3)(η^2-NO_3)]. In general, the spectra of these three hydrotris(pyrazolyl)borate complexes are characterized by two weak bands with an ϵ of 100−150 M^{-1} cm^{-1} in the NIR region (bands 1 and 3). These correspond to two negative features in the MCD spectrum. Note that band 3 is the strongest feature in the MCD spectra of all three compounds. Therefore, bands 1 and 3 can be assigned to d−d transitions. Besides these features, two additional bands also appear in the NIR region (bands 2 and 4), which, however, are both weak in absorption and MCD. Based on the calculations described below, these two transitions nevertheless correspond to the two remaining d−d transitions. At higher energy, two characteristic negative bands are observed between 20 000 and 26 000 cm^{-1} in the MCD spectra (bands 5 and 6). The corresponding absorption bands have ϵ of 150−400 M^{-1} cm^{-1}. Their origin is discussed in section A.4. In

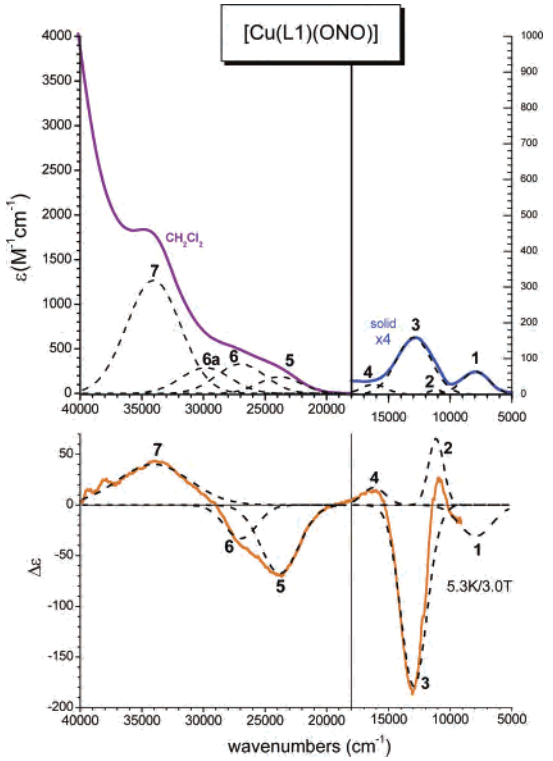

Figure 4. UV−vis absorption (top) and MCD spectrum (bottom) of **1**. The absorption spectrum in the UV−vis region was recorded in CH_2Cl_2 at low temperature; in the NIR region, the material was pressed between sapphire windows and recorded at 20K (see Experimental Section). The MCD spectrum was obtained on mulls. Also included are Gaussians obtained from a simultaneous fit of these data.

absorption, an intense feature appears between 30 000 and 35 000 cm^{-1} (band 7) with an ϵ of ∼1000 M^{-1} cm^{-1} for all compounds, which can therefore be assigned to a charge-transfer transition between copper(II) and the hydrotris(pyrazolyl)borate ligand.

A.4. Electronic Structure and Spectral Assignments. In order to obtain insight into the geometric and electronic properties of the species studied, DFT calculations were performed on a truncated version of the ligand $L1^-$, where all bulky substituents were removed. In order to provide a systematic comparison, the calculations were performed on both copper(I) and copper(II) oxidation states. Geometry optimizations were started from structures containing the conceivable coordination modes of nitrite to a mononuclear copper center, namely bidentate O-bound, monodentate O-bound, and monodentate N-bound (cf. Chart 1) giving rise to six models **1a**−**f** (Figure 5).

Geometric Structures and Energies. The optimized structures (BP86/TZVP) of the six models **1a**−**f** are shown in Figure 5. Table 5 lists calculated properties for these systems. Comparison can be made between the crystal structure of **1** and the bidentate Cu(II) species **1d**. In general, the calculations faithfully reproduce this structure. There is excellent agreement between theory and experiment for the metal−ligand bond distances with deviations being only on the order of 2−3 pm. Considering an effective C_{4v} symmetry (vide infra), the axial ligand field features a long $Cu-N_{ligand}$ bond of 2.110 Å experimentally which is overestimated in the calculations (predicted: 2.178 Å). However, all equatorial distances to the nitrogens and oxygens are in excellent agreement with experiment. Compared to free NO_2^- the predicted N−O distances are very similar (within 1 pm), and the nitrite molecule remains essentially symmetric in the optimized structure. The N−O distances of ∼1.28−1.29 Å are considerably longer than for $\cdot NO_2$. Thus, already the structure indicates limited charge transfer from NO_2^- to Cu(II) in **1d** and by inference also for the real complexes **1** and **2**.

At the B3LYP level, the relative energies including zero-point vibrational energies, thermal corrections, and solvation energies calculated using the COSMO model with a dielectric constant of 9.1 of the three coordination modes for the Cu(II) species (**1d**−**f**) show that the bidentate coordination mode is the preferred one (cf. Table 5). The N-bound species (**1e**) is predicted 5.5 kcal/mol higher in energy, while the monodentate O-bound species (**1f**) is isoenergetic with **1d**. For the Cu(I) species, the situation is even more complicated since all three coordination modes are predicted to be isoenergetic within ∼1 kcal/mol. However, in this case, it is not evident that a bidentate coordination mode exists as a separate minimum on the potential energy surface, and structures **1a** and **1c** are identical within the numerical scatter of the geometry optimization procedure. It is however, clear, that the N-bound coordination mode (**1b**) becomes energetically increasingly feasible for Cu(I) species, which is in agreement with the experimental findings in the literature (cf. Introduction). Importantly, the calculations suggest that this bonding mode is also possible in the Cu(II) species since the energetic penalty of only 5.5 kcal/mol may be overcome in a suitable ligand environment. The structural changes in going from the Cu(II) to the Cu(I) species are relatively limited. In general, the metal−ligand distances increase slightly, which is expected. The N−O bond distances also increase on average indicating a limited degree of back-bonding into the NO_2^- π^* orbital—a mechanism which has been held responsible for many of the interesting reactive features of nitrite bound to low-spin Fe(II) in the reaction cycle of cytochrome *c* nitrite reductase.[3] In the case of copper, the N-bound species in the Cu(I) state (**1b**) leads to N−O bonds which are still essentially equivalent and therefore have a formal bond order of 1.5 while the O-bound species (**1c**) naturally leads to significant asymmetry in the nitrite molecule giving rise to an essentially single N−O bond for the bonding oxygen and a bond with essentially N═O double bond character for the remote oxygen. These differences in bonding modes therefore represent quite different electronic structures which must be reflected in their associated reactivities. The differences are nicely reflected in the calculated diatomic N−O force constants in Table 5. According to the calculations the O-bound mode in the Cu(I) species is the only one which leads to a sizable activation of one of the two N−O bonds where the force constant goes down to ∼3.9 mdyn/Å, while the calculations on the free NO_2^- molecule yield a force constant of ∼5.7 mdyn/Å, quite similar to the values calculated for the N-bound species. Interestingly, this trend is reversed for the copper(II) complexes: here, the N-bound model system (**1e**)

Table 4. Results of the Simultaneous Gaussian Fit of the Absorption and MCD Spectra of the Compounds [Cu(L1)(η^2-ONO)], [Cu(L3)(η^2-ONO)], and [Cu(L3)(η^2-NO_3)]

	[Cu(L1)(η^2−ONO)] (**1**)					[Cu(L3)(η^2−ONO)] (**2**)					[Cu(L3)(η^2−NO_3)]				
band	ν_{max} (cm^{-1})	ϵ_{max} ($M^{-1}\,cm^{-1}$)		$\Delta\epsilon$ [T^{-1}]	f [a]	ν_{max} (cm^{-1})	ϵ_{max} ($M^{-1}\,cm^{-1}$)		$\Delta\epsilon$ [T^{-1}]	f [a]	ν_{max} (cm^{-1})	ϵ_{max} ($M^{-1}\,cm^{-1}$)		$\Delta\epsilon$ [T^{-1}]	f [a]
1	**7938**	63.2	Q[b]	−10.3	0.0008	**7931**	107.0	Q[b]		0.0011	**8245**	118.8	Q[b]		0.0011
2	11153	12.9	Q[b]	22.0	0.0001	9903	26.5	Q[b]	?	0.0002	10703	13.5	Q[b]	21.6	0.00004
3	**12950**	159.2	Q[b]	−59.7	0.0024	**11960**	142.6	Q[b]	−74.4	0.0019	**12183**	157.5	Q[b]	−78.1	0.0023
4	16197	27.9	Q[b]	5.7	0.0003	14900	25.8	Q[b]	4.7	0.0003	15062	27.2	Q[b]	7.8	0.0004
4a						18096	68.5	Q[b]	−10.2	0.0008					
5	**23799**	186.4		−22.5	0.0035	**21450**	134.4		−30.7	0.0027	**21864**	383.3[c]		−21.1	0.0090
6	**26977**	329.4		−11.1	0.0070	**23652**	299.6		−16.7	0.0058	**25342**	165.8[c]		−11.6	0.0025
6a	29825	288.9			0.0063	26889	334.3		5.2	0.0065	28420	404.8[c]			0.0082
7	**34043**	1267.7		13.4	0.0299	**31450**	744.1		6.2	0.0167	**33188**	1034.3[c]		14.0	0.0251
8						33769	1279.1		?	0.0266	35505	355.6[c]		−14.2	0.0083
9											39336	1913.4[c]			0.0397

[a] f: oscillator strength. [b] Q: fit of the solid-state UV−vis spectra; the other band positions are obtained from the low-temperature solution UV−vis spectra (in CH_2Cl_2). For [Cu(L3)(η^2-NO_3)], UV−vis spectra recorded in a KBr disk were used instead of the solution data. [c] The intensities of these bands are probably overestimated due to the scattering background of the KBr disk that becomes significant at low wavelengths.

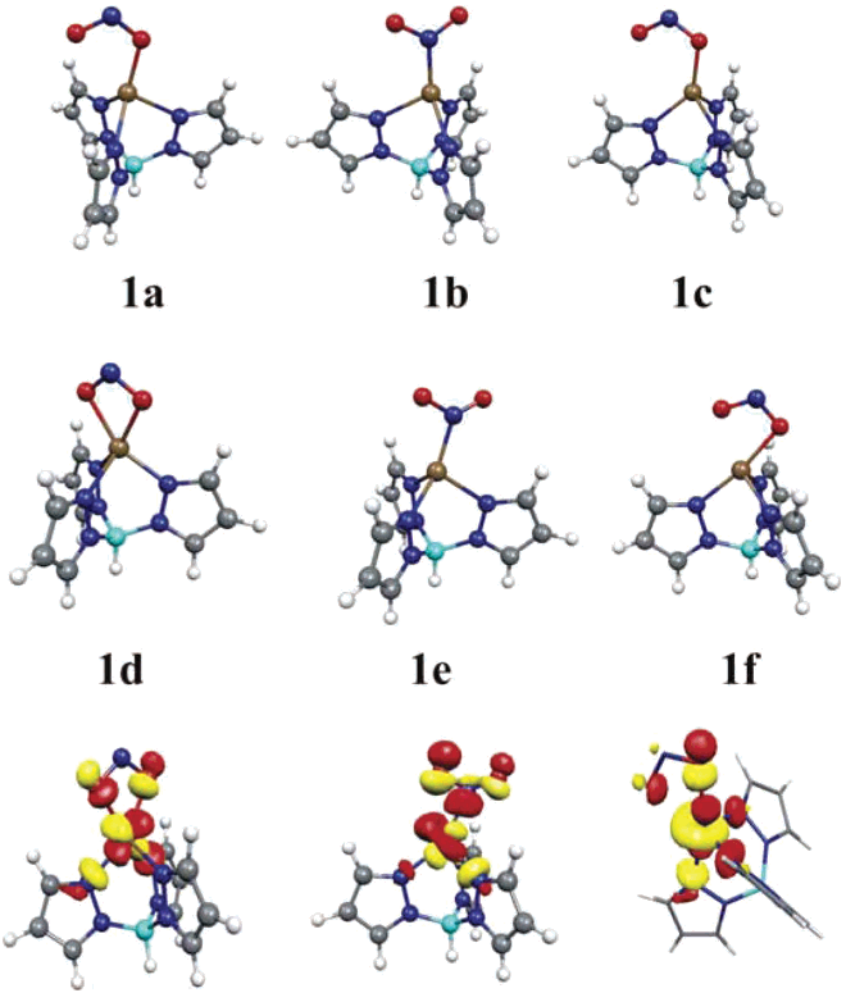

Figure 5. Optimized geometries (BP86/TZVP) for Cu(I)−nitrite species **1a**−**c** and Cu(II)−nitrite species (**1d**−**f**) together with the calculated SOMOs (B3LYP/TZVP) for species **1d**−**f**. Metric parameters are collected in Table 5.

shows large anisotropy of the N−O bonds, whereas these have similar force constants for the O-bound isomers **1d** and **1f**.

Electronic Structure. The SOMOs for the three Cu(II) species (**1d**−**f**) are also included in Figure 5. From an electronic point of view it becomes evident that the coordination sphere of **1d** should be considered as a square pyramid with the plane being spanned by the two oxygens and two pyrazolyl-nitrogens. This leads to the Cu-$d_{x^2-y^2}$ based singly occupied MO which is strongly σ-antibonding to the ligand. This electronic structure changes drastically upon going to the monodentate species **1f** where the SOMO is clearly of the d_{z^2} type and oriented toward the axial ligands. This is in excellent agreement with the EPR results obtained for complexes **1** and **2** where the asymmetric binding mode of nitrite in **2** leads to a d_{z^2} ground state. Yet another type of

Table 5. Calculated Relative Energies (B3LYP/TZVP+ZPE,COSMO(water)), Metrical Parameters (BP86/TZVP), NBO Spin-Populations (B3LYP/TZVP,COSMO(water)), and Quasi-Diatomic Force Constants (BNP86/TZVP) for Models **1a**−**f**

	1a	**1b**	**1c**	**1d**	**1e**	**1f**
energy[a]	1.2	0.9	0.0	0.0	5.5	0.1
R(Cu−O_1)	1.974	2.788	1.982	2.050	2.486	2.057
R(Cu−O_2)	2.859	2.816	2.905	2.063	2.908	2.051
R(Cu−N_1)	2.843	1.934	2.887	2.503	1.925	2.501
R(Cu−N_{pz})[b]	2.073	2.155	2.092	2.035	2.021	1.999
R(Cu−N_{pz})[c]	2.248	2.068	2.177	2.178	2.108	2.177
∠(O−N−O)	115.6	118.4	118.0	110.0	125.7	109.9
spin-Cu[d]				0.651	0.495	0.651
f_{NO}[e]	3.91/7.04	5.92/6.03	3.96/6.96	5.15/5.07	8.05/5.97	5.17/5.07

[a] Relative energy in kcal/mol: the lowest energy for the Cu(I) species (a−c) and Cu(II) species (d−f) is taken as the zero-point. [b] Equatorial nitrogen. [c] Axial nitrogen. [d] Spin population on copper according to the NBO analysis. [e] Quasi-diatomic N−O force constants in mdyn/Å.

Table 6. Calculated Absorption Spectrum of **1d** (B3LYP/TZVP) in Water (ϵ=80.4, Refractive Index=1.33) as Modeled by the COSMO Model[a]

transition energy (cm^{-1})	f_{osc} ($\times 10^4$)	transition
7135	6.8	Cu-d_{z^2}→Cu-$d_{x^2-y^2}$
12 248	26.5	Cu-d_{xz}→Cu-$d_{x^2-y^2}$
13 669	4.4	Cu-d_{yz}→Cu-$d_{x^2-y^2}$
15 395	3.2	Cu-d_{xy}→Cu-$d_{x^2-y^2}$
17 910	1.1	N_{pz}-π→Cu-$d_{x^2-y^2}$
22 180	20.0	N_{pz}-π→Cu-$d_{x^2-y^2}$
23 534	13.4	NO_2^--σ_1→Cu-$d_{x^2-y^2}$
25 316	25.7	NO_2^--σ_1+ N_{pz}−π→Cu-$d_{x^2-y^2}$
28 574	31.1	N_{pz}-π→π^*
29 589	19.2	N_{pz}-π→π^*
30 734	16.7	N_{pz}-π→π^*
30 836	37.7	N_{pz}-π→π^*
31 652	498.0	NO_2^--π→Cu-$d_{x^2-y^2}$
32 522	620.2	NO_2^--σ_2→Cu-$d_{x^2-y^2}$

[a] Only transitions of d−d character or with calculated oscillator strengths larger than 10^{-3} are listed.

SOMO is calculated for the N-bound species (**1e**). In this case, the SOMO resembles that of **1d** in that it is localized essentially in a trigonal plane but with a strong contribution (∼33%) from the σ-HOMO of the nitrite ligand (with significant contributions of the nitrogen lone pair) and a correspondingly reduced contribution (46%) from Cu(II). This much stronger σ-donor character of the NO_2^- in the N-bound structure is also seen in the results of the natural population analysis which suggests a reduced positive charge and spin population on the copper (65.1% spin population on Cu in **1d** compared to only 49.5% in **1e**). Likewise, the Löwdin bond order of the Cu−N bond in **1d** (0.66) is much stronger than that of the Cu−O bonds in **1c** (0.49). In all binding modes it is observed that the Cu−nitrite bond becomes stronger in the Cu(I) forms (Cu−N bond order 0.75 in **1b** and Cu−O bond order 0.61 in **1a**).

Electronic Spectra. The interpretation of the optical absorption spectra (Figure 4, Table 4) in the d−d-region of **1** are straightforward based on the combination of absorption and MCD measurements together with TD-DFT (B3LYP/TZVP) calculations. As pointed out above, the combination of theory and experiment reveals that the effective site symmetry is close to C_{4v}. Thus, the first transition which is expected leads from the Cu-d_{z^2} based MO to the Cu-$d_{x^2-y^2}$ based SOMO. This transition is observed at 7983 cm^{-1} and calculated at 7135 cm^{-1} (Table 6). It is associated with a negative MCD C-term. In the computations the d_{z^2} orbital mixes strongly and accidentally with an energetically nearby NO_2^- in-plane lone pair orbital which renders the calculated transitions somewhat unclear (Figure 6). However, the transition should certainly be assigned to a d−d transition. The next two bands can safely be assigned to transitions from the Cu-$d_{xz,yz}$ based MOs to the SOMO. They are, as expected, associated with a derivative shaped MCD signal. The two transitions are calculated at 12 248 cm^{-1} and 13 669 cm^{-1} which is very close to the observed transition energies of 11 153 cm^{-1} and 12 950 cm^{-1}. However, the precise order of the two states is not perfectly clear since one of them (band 3) is much more intense than the other one. This is reproduced by the calculations which, however, give the much stronger transition (f_{calc}=0.0026) lower in energy than the weaker one (f_{calc}=0.0003), which is opposite to the experimental observation (band 2: f_{exp}=0.0001 and band 3: f_{exp}=0.0024). Since these two transitions are very close in energy, this error can certainly be tolerated. Finally, the fourth d−d transition corresponds to the d_{xy} to $d_{x^2-y^2}$ transition which is calculated at 15 395 cm^{-1} and observed as a positive C-term at 16197 cm^{-1} (Table 4), again in excellent agreement with experiment. The assignments of the d−d transitions are illustrated in Figure 6.

The interpretation of the more intense transitions starting from ∼23 000 cm^{-1} experimentally is less straightforward. They must belong to charge-transfer transitions, which are, however, not obviously associated with the nitrite ligand as pointed out above. For charge-transfer transitions TD-DFT calculations are somewhat problematic due to the self-interaction error which tends to give much too low energies for such transitions. The problem is somewhat reduced with hybrid density functionals since these are closer to being self-interaction free, but we have also observed shortcomings in this respect in a number of applications. Keeping these limitations in mind, the first transitions past the d−d region predicted by B3LYP/TD-DFT correspond to pyrazole-$\pi_{1,2}$ to Cu^{II} LMCT transitions which appear with moderate intensity ($f = 1.1 \times 10^{-4}$ and 20.0×10^{-4}) at 17910 and 22180 cm^{-1}. Second, there are calculated intraligand excitations with low intensity. It is noteworthy that the d−d transitions have negligible predicted solvent shifts (<100 cm^{-1}), while the solvent shift of the LMCT transitions is very large and amounts to a downshift of 3000−6000 cm^{-1}. The calculations also do predict nitrite to Cu^{II} LMCT transitions. The first two lead from the high-lying nitrite-

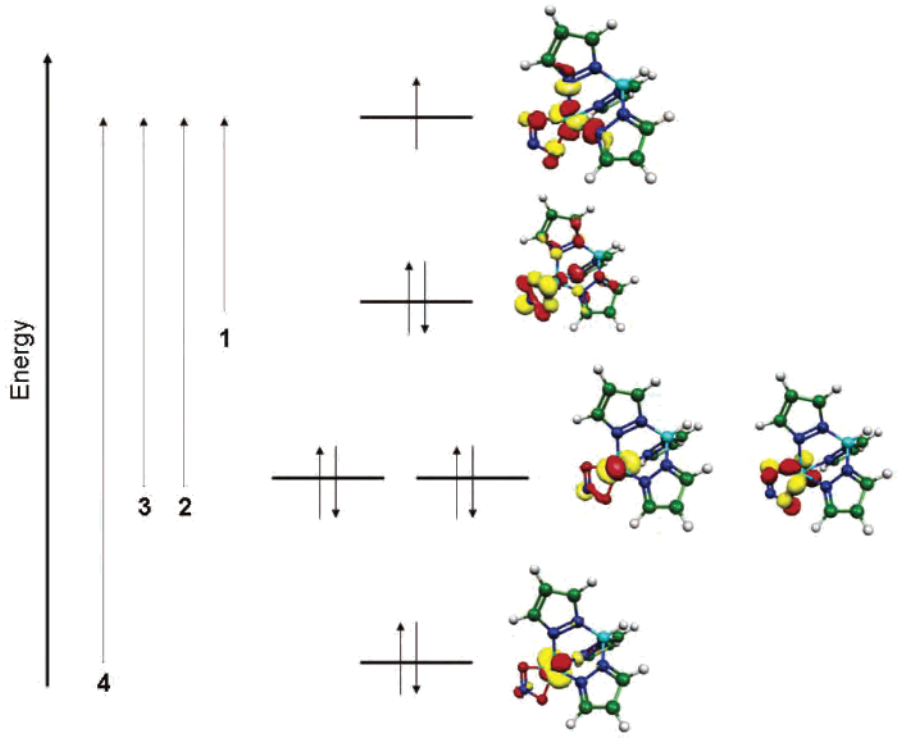

Figure 6. Interpretation of d−d transitions in **1** in terms of one-electron transitions.

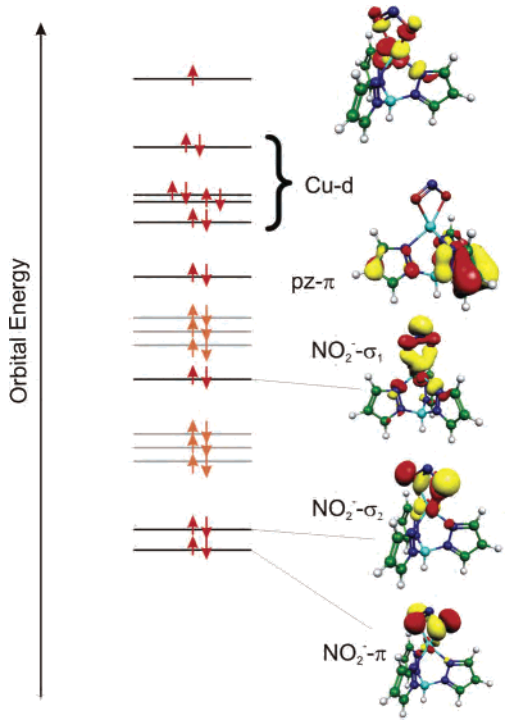

Figure 7. Important orbitals for the interpretation of the LMCT region of **1** calculated for **1d**.

HOMO (NO_2^--σ_1; cf. Figure 7) to the SOMO and are calculated as a pair at 23 534 cm^{-1} ($f = 13.4 \times 10^{-4}$) and 25 316 cm^{-1} ($f = 25.7 \times 10^{-4}$). Both show (accidental) mixing with pyrazole-π to Cu^{II} LMCT transitions, which is probably the source of intensity of these two absorption features. A pair of high-intensity nitrite nonbonding σ_2 and π (the HOMO-1 and HOMO-2 of free nitrite; see also Figure 7) to Cu(II) LMCT transitions is predicted to occur at 31 652 cm^{-1} and 32 522 cm^{-1} with oscillator strengths of 498.0×10^{-4} and 620.2×10^{-4}, respectively. The primary intensity of these bands relates to the σ_2-LMCT transition which has a large transition dipole moment due to the good overlap of the corresponding σ_2 orbital (cf. Figure 7) with the SOMO of copper(II), while the π-transition is inherently weak and borrows its intensity from the σ_2-transition. It is difficult to unambiguously judge the reliability of these calculations with respect to the CT features. Broadly speaking, bands 4−6 of **1** (cf. Figure 4) are of moderate intensity and occur around 20 000−30 000 cm^{-1} close to the energy region where the moderate intense LMCT transitions are predicted. But detailed assignments are not possible. A high-intensity feature which is associated with a low-intensity positive MCD C-term feature (band 7) is observed around ∼35 000 cm^{-1} which is ∼3000 cm^{-1} higher in energy than predicted for the σ_2 and π to Cu(II) LMCT. Hence, the evidence for assigning band 7 to a nitrite to Cu^{II} LMCT transition is ambiguous and awaits the collection of UV resonance-Raman data which is unfortunately outside the possible excitation range of the equipment available to us.

B. Copper(II)−Nitrito Complex with Tris(pyrazolyl)-methane Coligand (3). B.1. Synthesis. The reaction of [Cu(L1′)Cl_2] with 2 equiv of $NaNO_2$ in the mixed dichloromethane/methanol solvent at room temperature readily gives the corresponding copper(II)−nitrito complex **3** following eq 2. Preliminary crystallographic data shown in Figure S2 indicate a very unusual binding mode of the two nitrite ligands in this complex where one nitrite shows monodentate coordination via one oxygen atom, whereas the other nitrite is N-bound. Only a few complexes are known in the literature that exhibit this mixed O/N coordination of

Table 7. Comparison of Experimental and Calculated Vibrational Frequencies of Cu(II)−$(NO_2^-)_2$ Complexes

		vibration							
		ν^N(N−O)		ν^O(N−O)		δ(O−N−O)			
compound[a]		ν_{as}	ν_s	N═O	N−O	δ_s	δ_{as}	ν^O(Cu−O)	ν^N(Cu−N)
[Cu(L1′)(η^1-ONO)(NO_2)] (**3**)	IR	1402	1141 ?		1060			352	223
[Cu(L1′)(η^1-O^{15}NO)($^{15}NO_2$)]	IR		∼1115 ?	1353	1053			345	220
[Cu(L1′)(η^1-ONO)(NO_2)] − calc ($\tilde{\mathbf{3}}$)		1421	1254	∼1380	1029	798	768	320	213/211

		vibration							
		ν(N−O^{nb})		ν(N−O^b)		δ(O−N−O)		ν_s(Cu−O)	
compound[a]		ν_{as}	ν_s	ν_s	ν_{as}	δ_s	δ_{as}	ν_s	ν_{as}
[Cu(L1″)(η^1-ONO)$_2$] (**4**)	IR	1346		1182		851		378	348
	R		1325	1190/1176		853	804	380	351
[Cu(L1″)(η^1-O^{15}NO)$_2$]	IR	1321		1156		844		374	344
	R		1299	1161		847	797	372	344
[Cu(L1″)(η^1-ONO)$_2$] − calc ($\tilde{\mathbf{4}}$)		1337	1349	1106	1058/1054	799	786	358	335

[a] Models $\tilde{\mathbf{3}}$ and $\tilde{\mathbf{4}}$ used for the calculations are described in the Experimental Section.

two nitrite ligands.[36] Further work is in progress to obtain

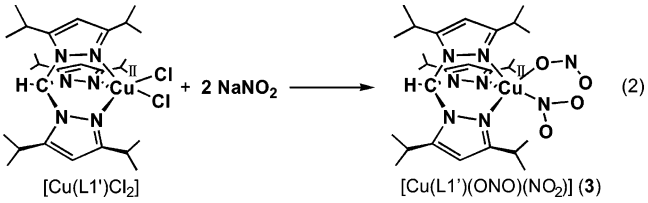

(2)

better crystals of **3** to confirm this result. Spectroscopic data suggest that the nitrogen atoms of the tris(pyrazolyl)methane ligand bind to the copper(II) center in a facially coordinating tridentate mode in agreement with the structural data.

B.2. Vibrational Spectra and Assignments. The IR spectrum of [Cu(L1′)(ONO)(NO_2)] (**3**) is shown in Figure S6 together with that of the corresponding $^{15}NO_2^-$ isotope labeled complex. As one can see, the B−H stretch around 2500 cm^{-1} is absent in the spectra in accordance with the presence of the tris(pyrazolyl)methane ligand in **3**. Due to the coordination of two nitrite ligands, the number of vibrations increases which makes the assignments more complicated. From the preliminary crystal structure of **3**, the binding mode of nitrite is different in this complex compared to [Cu(L1′)(η^1-NO_3)$_2$] and [Cu(L1″)(η^1-ONO)$_2$] (vide infra) which both show two η^1-O coordinated nitrate and nitrite ligands, respectively. Calculations on a large model system for **3** which includes the isopropyl substituents facing the nitrite binding site ($\tilde{\mathbf{3}}$; see Experimental Section) show that the local vibrations of the two bound nitrite units are basically localized and do not mix significantly (with exception of the O−N−O bending mode) in this complex. In agreement with the calculations on the hydrotris(pyrazolyl)borate model complexes **1d**−**f** (vide supra), the results for $\tilde{\mathbf{3}}$ predict that N-bound nitrite shows the antisymmetric N−O stretch at much higher energy (>1400 cm^{-1}) compared to the O-bound isomers. Based on this, ν_{as}^N(N−O) of the N-bound nitrite in **3** is assigned to the isotope sensitive band at 1402 cm^{-1} that is absent in the $^{15}NO_2^-$ complex. This feature probably shifts into the intense band at about 1380 cm^{-1} (cf. Figure S6). As shown in Table 7, this mode is predicted at 1421 cm^{-1} for $\tilde{\mathbf{3}}$ in very good agreement with experiment. The calculations on $\tilde{\mathbf{3}}$ also show that the O-bound nitrite is strongly polarized in this complex such that the N−O bond of the copper-bound oxygen is long and has single bond character (bond 1 in Chart 2, top), whereas the other N−O bond is short (bond 2 in Chart 2, top) and can be regarded as a (weak) N−O double bond. The two corresponding stretching vibrations, ν^O(N−O) (bond 1) and ν^O(N═O) (bond 2), only weakly interact. In the IR spectra of the $^{15}NO_2^-$ isomer of **3**, a new band appears at 1353 cm^{-1}, which is assigned to ν^O(N═O). To lower energy, two isotope sensitive bands are found at 1141 cm^{-1} and 1060 cm^{-1} (cf. Table 7). The feature at 1141 cm^{-1} is assigned to ν_s^N(N−O) of the N-bound isomer, although this mode shows an unusually large deviation from the calculated frequency of 1254 cm^{-1} in Table 7, and, hence, this assignment is only tentative. The band at 1060 cm^{-1} corresponds to ν^O(N−O) of the O-bound isomer (bond 1). The calculated frequency of 1029 cm^{-1} for this mode is in very good agreement with experiment. The O−N−O bending mode that is quite intense in the hydrotris(pyrazolyl)borate compounds cannot be identified in the spectra of **3**. The reason for this is unclear. In the FIR region, the Cu−O stretch of the O-bound nitrite ligand is observed at 352 cm^{-1} showing a shift to 345 cm^{-1} in the ^{15}N labeled compound, which is very similar in energy to **1** and **2**. This mode is calculated at 320 cm^{-1} for $\tilde{\mathbf{3}}$. Finally, the Cu−N stretch of the N-bound nitrite appears at very low energy (223 cm^{-1}), which is probably related to strong mixing of this mode with the O−N−O bend. Unfortunately, no Raman spectra could have been determined for **3** due to luminescence problems.

B.3. Electronic Spectra. Figure 8 shows the absorption and MCD spectra of complex **3** together with Gaussians obtained from a simultaneous fit of the data. Band positions and extinction coefficients are listed in Table 8. In comparison with the spectra of complexes **1** and **2** described above,

(36) (a) Lott, A. L., II. *J. Am. Chem. Soc.* **1971**, *93*, 5313−5314. (b) For, purely inorganic compounds, see, for example: Klanderman, K. A.; Hamilton, W. C.; Bernal, I. *Inorg. Chim. Acta* **1977**, *23*, 117−129.

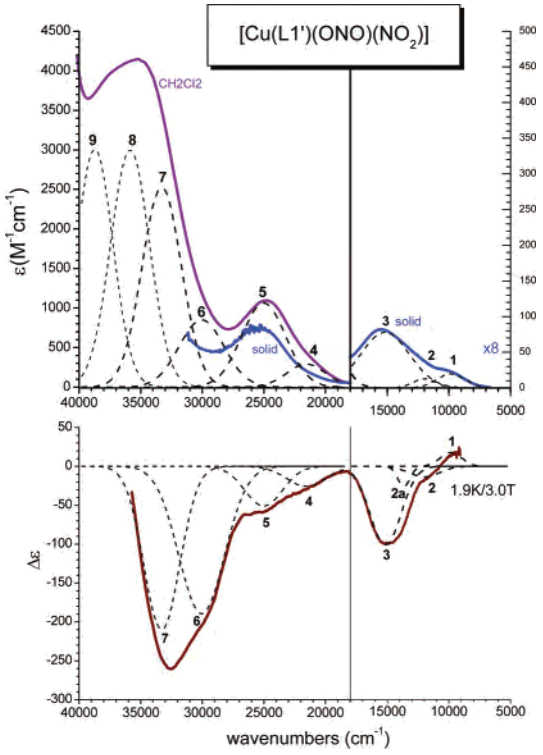

Figure 8. UV−vis absorption (top) and MCD spectrum (bottom) of **3**. The absorption spectrum in the UV−vis region was recorded in CH_2Cl_2; in the NIR region, the material was pressed between sapphire windows and recorded at 20K (see Experimental Section). The MCD spectrum was obtained on mulls. Also included are Gaussians obtained from a simultaneous fit of these data.

Chart 2

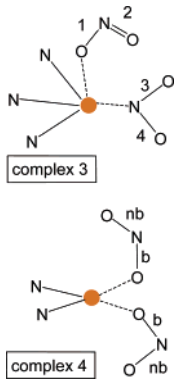

the region below 30 000 cm^{-1} looks quite similar with essentially four intense transitions (in this case bands 1, 3, 4, and 5). Especially the MCD intensity of these bands fits quite well with the corresponding bands in the other complexes as shown in Table 8. Hence, these features are also assigned to the four d−d transitions of copper(II) (bands 1, 2, 2a, and 3) and CT transitions as described in section A.4. Compared to **1** and **2**, the change in coordination environment in **3** is reflected by a change of the MCD intensity pattern of the d−d transitions, which indicates a different energy sequence of the d orbitals in this complex. Nevertheless, the occurrence of the highest energy d−d band around 15 000 cm^{-1} in the MCD spectrum indicates a square pyramidal coordination geometry for this compound, in

Table 8. Results of the Simultaneous Gaussian Fit of the Absorption and MCD Spectra for Compound [Cu(L1′)(η^1-ONO)(η^1-NO_2)] (**3**)

band	ν_{max} (cm^{-1})	ϵ_{max} ($M^{-1}\,cm^{-1}$)		$\Delta\epsilon$ [T^{-1}]	f [a]
1	**9832**	19.7	Q[b]	5.9	0.0002
2	11 985	12.6	Q[b]	−4.5	0.0001
2a	13 651			−8.7	
3	**15 148**	77.8	Q[b]	−33.7	0.0017
4	**21 566**	290.3		−8.5	0.0050
5	**25 018**	1064.1		−17.0	0.0206
6	30 048	850.2		−63.3	0.0167
7	33 286	2528.9		−70.1	0.0436
8	35 854	3000.5			0.0512
9	38 721	3008.9			0.0469

[a] f: oscillator strength. [b] Q: fit of the solid-state UV−vis spectra; the other band positions are obtained from the low-temperature UV−vis spectra in CH_2Cl_2 solution.

agreement with the preliminary X-ray structural data.[37] TD-DFT calculations on model $\tilde{\mathbf{3}}$ predict d−d transition energies of 8472, 11 913, 14 420, and 15 007 cm^{-1}, which is in good agreement with experiment (cf. Table 8). The fully optimized structure of $\tilde{\mathbf{3}}$ is somewhat intermediate between square pyramidal and trigonal bipyramidal, which explains the remaining deviations of these numbers from experiment. To higher energy, mixed pyrazole-π to Cu^{II} and nitrite to Cu^{II} LMCT transitions (into the SOMO of copper) of medium intensity are calculated at 19 462, 24 242, 24 534, and 24 940 cm^{-1} ($f = 100 \times 10^{-4}$−1000×10^{-4}). Detailed assignments of the observed bands are not possible. No transitions of significant intensity are calculated between 25 000 and 30 000 cm^{-1} in accordance with experiment. In summary, these spectral assignments are in good agreement with the results for **1** (vide supra). The low-energy CT region of these compounds is most probably dominated by pyrazole-π to Cu(II) CT, which would explain why the spectra of all compounds investigated here are quite similar below 30 000 cm^{-1}. Note that the calculated larger oscillator strengths for $\tilde{\mathbf{3}}$ compared to **1d** are in agreement with experiment. Important differences between **3** and **1** occur in the higher energy region of the spectra: two bands are observed at 30 048 and 33 286 cm^{-1} (bands 6 and 7) for **3** which are intense in absorption as well as MCD. No other compound including **4** (vide infra) has corresponding spectral features. One possible explanation is that this difference relates to the fact that compound **3** is the only complex in this series including **4** (vide infra) that has an N-bound nitrite; in all other cases, the nitrite is O-bound. Hence, these bands would then be associated with a nitrite to copper charge-transfer transition that does only occur for the N-bound isomer. However, from the TD-DFT calculations, there is no evidence for such spectral features. In fact, the calculations show only one band of corresponding intensity at 31 018 cm^{-1} ($f = 420 \times 10^{-4}$), which, however, again corresponds to mixed pyrazole-π to Cu^{II} and nitrite to Cu^{II} LMCT. From the calculations, the N-coordination mode of nitrite does not have a significant effect on the optical spectra. However,

(37) From the structural data of **3**, the τ value is 0.04, which corresponds to a square pyramidal geometry (N11−Cu1−O43=169.2 deg, N31−Cu1−N21=171.7 deg, apical position occupied by N21). This is also in agreement with the EPR spectrum, which shows the usual d_{x2-y2} ground state for this coordination geometry.

the rather poor agreement between the calculated and experimental spectra in the region >30 000 cm^{-1} renders this conclusion somewhat ambiguous, and, hence, the origin of the 30 048 and 33 286 cm^{-1} features of **3** remains unclear.

For comparison, absorption and MCD data of the corresponding nitrato complex [Cu(L1′)(η^1-NO_3)$_2$] are shown in Figure S9. Importantly, in this case the MCD data recorded in a mull do not line up with the absorption spectra recorded in solution, KBr, or between sapphire windows although the overall appearance of the spectra is quite similar. The reason for this observation is not entirely clear. One possibility is that some kind of isomerization of the complex takes place in solution and during the preparation of the KBr disk. In addition, during the measurement of the MCD data it was noticed that this complex is photolabile. Therefore, the optical spectra of [Cu(L1′)(η^1-NO_3)$_2$] are not further analyzed because they are under severe doubt.

C. Copper(II)−Nitrito Complex with Bis(pyrazolyl)-methane Coligand (4). C.1. Crystal Structure. Treatment of [Cu(L1″)Cl_2] with 2 equiv of $NaNO_2$ yields the nitrito complex **4** as shown in eq 3. On the other hand, the reaction between $Cu(NO_3)_2 \cdot 3H_2O$ and L1″ in a mixed acetone/

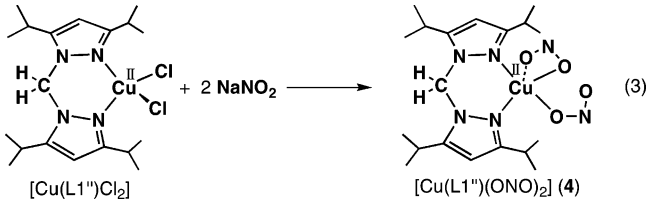

(3)

dichloromethane solvent at room temperature readily gives the corresponding copper(II)−nitrato complex **5** in high yield. The single crystal structural results for **4** and **5** confirm that the nitrogen atoms of L1″ bind to the copper(II) ions in a facially bidentate coordination mode forming mononuclear structures. These structures are shown in Figures 7 and S1, respectively. Because these complexes are neutral, the oxidation state of the copper is +II in both cases. Complex **4** consists of a copper center with two pyrazolyl nitrogen atoms (N11 and N21) and two oxygen atoms of the two nitrite ions (O31 and O41) bound. In addition, there is a weak interaction between Cu(II) and a third nitrite oxygen (O42) at a distance of 2.370(3) Å as shown in Figure 7. Including this weak Cu−O interaction, a square pyramidal coordination geometry around the copper(II) is obtained. The O32 atom is 2.408(2) Å away from the metal. The total angle around the copper(II) ion is 362.08°. The deviation of the copper(II) ion from the corresponding N_2O_2 plane in the apical direction is 0.10(1) Å. In the case of the nitrato complex **5**, the coordination geometry around the copper(II) ion is essentially square planar. This can also be understood from the total angle (361.67°) around the copper(II) center and the deviation (0.10(1) Å) of the copper(II) ion from the corresponding N_2O_2 plane formed by the two pyrazolyl nitrogens (N11 and N21) and two nitrate oxygens (O31 and O41) in the apical direction. One of the nitrate ligands is located above and the other one below the N_2O_2 plane (cf. Figure S1), exhibiting long Cu1−O32 and

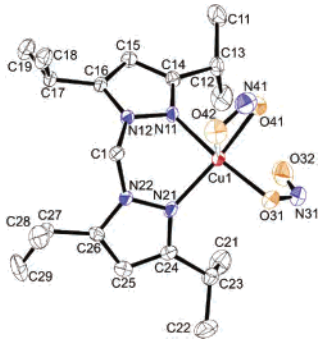

Figure 9. Crystal structure of [Cu(L1″)(η^1-$ONO)_2$] (**4**) (50% probability ellipsoids shown).

Cu1−O42 distances of 2.407(2) and 2.497(2) Å, respectively. This geometry is due to the steric hindrance of nitrate and the L1″ ligand, which is minimized this way.

C.2. Vibrational Spectra and Assignments. From the crystal structure of **4**, it is known that both nitrite ligands can be considered essentially η^1-O bound. Calculations on the η-O bound isomers **1d**,**f** of the hydrotris(pyrazolyl)borate complex (vide supra) indicate that the weak interaction of O42 with copper is most likely not relevant for the vibrational properties of **4**. To gain further insight, calculations on a large model system for **4** which includes the isopropyl substituents facing the nitrite binding site (**4̃**; see Experimental Section) have been performed. These calculations show that both nitrite ligands are polarized in **4**, i.e., the N−O bond of the coordinated oxygen (N−O^b) is longer than the remaining N−O bond (N−O^{nb}; cf. Chart 2). However, this polarization is clearly weaker than the one observed for the O-bound nitrite in **3** (vide supra). Nevertheless, it is significant enough to lead to an interesting vibrational coupling scheme of the four local N−O coordinates in **4**. Surprisingly, the calculations predict that vibrational coupling between the pairs of N−O^b and N−O^{nb} coordinates is dominant and not the coupling between the N−O coordinates of the individual nitrite ligands as would be expected. This leads to the observation of corresponding symmetric (ν_s) and antisymmetric (ν_{as}) combinations of N−O^{nb} and N−O^b, respectively (cf. Table 7). These predictions are supported by the experimental findings.

The IR and Raman spectra of [Cu(L1″)(η^1-$ONO)_2$] (**4**) are shown in Figures 10 and 11, respectively, together with the corresponding $^{15}NO_2^-$ isotope labeled data. The band at 1346 cm^{-1} in the IR spectrum that shifts to 1321 cm^{-1} in the $^{15}NO_2^-$ compound is assigned to one combination of the ν(N−O^{nb}) stretches. The second component is identified in the Raman spectrum at 1325 cm^{-1} showing a shift to 1299 cm^{-1} upon isotope labeling. The small energy splitting between these combinations of only 21 cm^{-1} reflects the fact that the N−O^{nb} bonds of the two nitrite ligands are separated by four bonds. This value is in good agreement with the calculations (predicted: 12 cm^{-1}). However, the fact that the 1346 cm^{-1} feature is IR active whereas the 1325 cm^{-1} mode is Raman active indicates that the band at higher energy should be assigned to the antisymmetric combination ν_{as}(N−O^{nb}), which is opposite to the order found in the calculations (cf. Table 7). At lower energy, an isotope

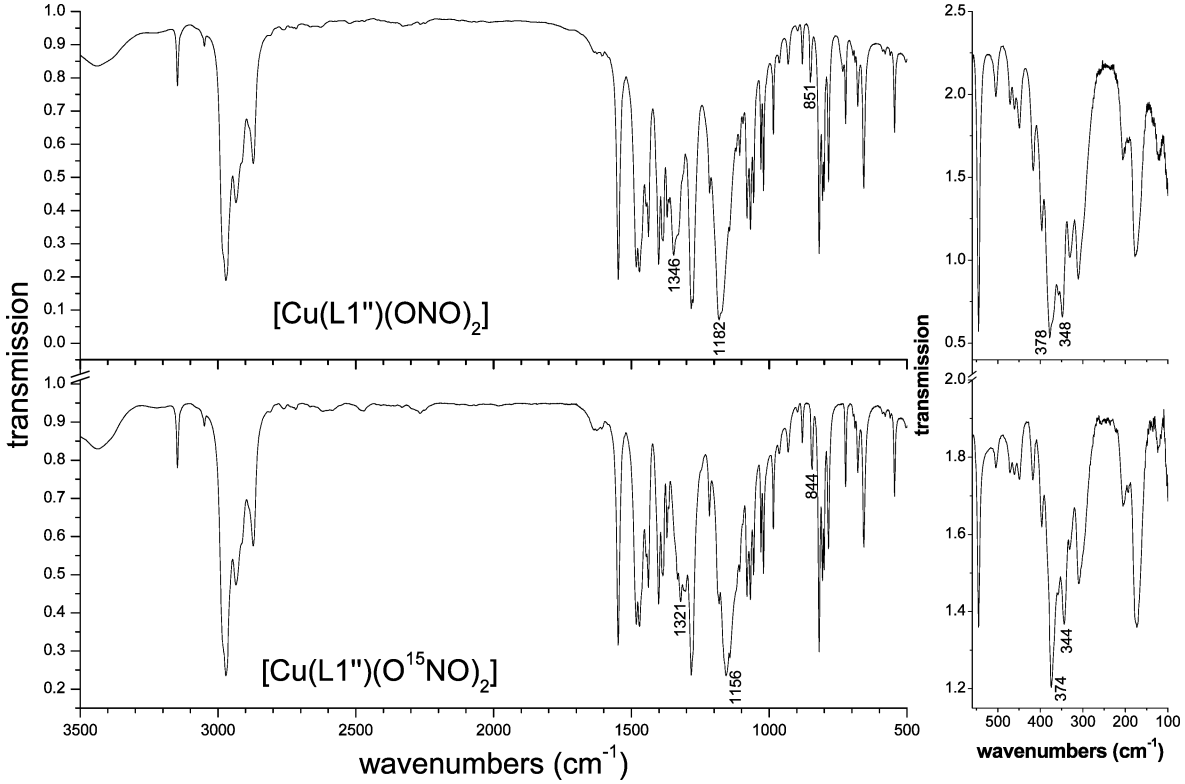

Figure 10. IR spectrum of **4** (top) and of the corresponding $^{15}NO_2^-$ isotope labeled complex (bottom).

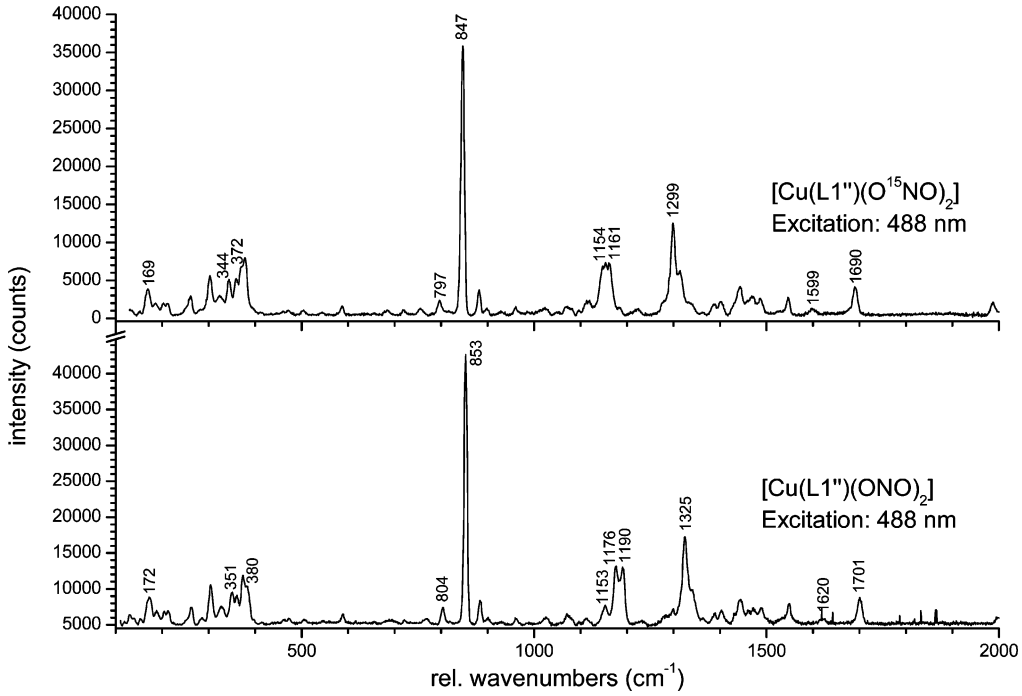

Figure 11. Raman spectrum of **4** (bottom) and of the corresponding $^{15}NO_2^-$ isotope labeled complex (top).

sensitive mode is observed at 1182 cm^{-1} in the IR spectrum that shifts to 1156 cm^{-1} upon ^{15}N labeling. This feature appears split in the Raman spectrum into two components at 1190 and 1176 cm^{-1}. Upon isotope substitution, one band is found at 1161 cm^{-1}. Since this mode is strongly IR and Raman active, it is assigned to $\nu_s(N-O^b)$ in agreement with the calculations (predicted: 1106 cm^{-1}). The fact that this mode appears split in the Raman spectrum is due to accidental mode mixing of $\nu_s(N-O^b)$ with a small band around 1185 cm^{-1}, which vanishes upon isotope labeling. From the calculations, the other component, $\nu_{as}(N-O^b)$, should appear about 50 cm^{-1} to lower energy (cf. Table 7). However, we were not able to identify this mode in the experimental spectra. One component of the O−N−O bending mode is identified with the isotope sensitive bands at 851 cm^{-1} in the IR spectrum. In the Raman data, this

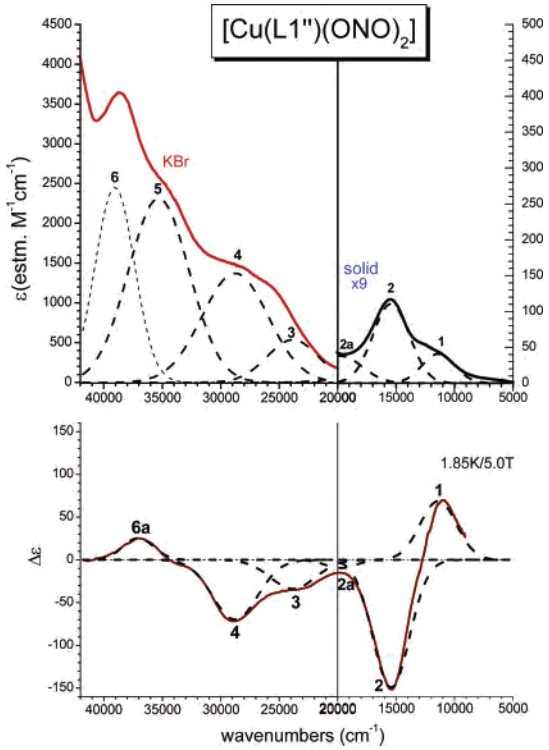

Figure 12. UV−vis absorption (top) and MCD spectrum (bottom) of **4**. The absorption spectrum in the UV−vis region was recorded in a KBr disk at 20K; in the NIR region, the material was pressed between sapphire windows and recorded at 20K (see Experimental Section). The MCD spectrum was obtained on mulls. Also included are Gaussians obtained from a simultaneous fit of these data.

feature is observed at 853 cm^{-1}. Surprisingly, this band is by far the most intense feature in the Raman spectra of **4** (at an excitation wavelength of 488 nm). Hence, this band is assigned to the symmetric combination of the two δ(O−N−O) coordinates. The corresponding antisymmetric mode is identified with the weak Raman feature at 804 cm^{-1}. In the FIR region, two bands are observed at 378 and 348 cm^{-1} that shift to 374 and 344 cm^{-1}, respectively, in the $^{15}NO_2^-$ complex. These are assigned to the symmetric and antisymmetric combinations of the two symmetric Cu−O stretches, respectively. These modes are also observed in the Raman spectra at comparable energies.

Besides these fundamentals, two more isotope sensitive bands are identified in the Raman spectra of **4** at 1701 and 1620 cm^{-1} (cf. Figure 11). The former is assigned to an overtone of the 853 cm^{-1} feature, whereas the latter must correspond to a combination mode, for example of the 1325 cm^{-1} feature with the (unassigned) metal−ligand vibration at 300 cm^{-1}. Altogether, a very detailed picture of the vibrational structure of the Cu(II)−$(ONO^-)_2$ unit is available for **4** due to the high quality of the obtained data.

C.3. Electronic Spectra. The UV−vis absorption and MCD data of compound [Cu(L1″)(η^1-ONO)$_2$] (**4**) are shown in Figure 12 together with the results of a simultaneous Gaussian fit of these data. In comparison, the spectra of the corresponding nitrato compound (**5**) are shown in Figure S10. In the case of **5**, absorption spectra recorded in solution and in KBr do not line up with the MCD and solid-state absorption data. This indicates that some kind of isomerization or rearrangement of the ligand sphere occurs upon solvatisation of the nitrato complex. This even occurs in a noncoordinating solvent such as dichloromethane as shown in Figure S10. For the UV−vis region, mull absorption spectra have therefore been recorded; however, the obtained quality of the data is rather poor which limits the interpretation. In general, the electronic spectra (especially MCD) of the Cu(II)−nitrato and −nitrito complexes with the same type of coligand L and O-bound nitrite are comparable in their overall appearance as already described above. This is also the case here for the nitrato and nitrito compounds with L1″. In the NIR region, two weak bands are observed (bands 1 and 2), which give rise to a pseudo-**A**-term signal in the MCD. Therefore, these are assigned to the Cu-d_{xz} to Cu-$d_{x^2-y^2}$ and Cu-d_{yz} to Cu-$d_{x^2-y^2}$ transitions. In the essentially square-planar coordination environment (plus the small Cu−O42 interaction) of complex **4**, the other d−d transitions are likely located at lower energy. One of them is probably identified with the weak absorption feature at 7507 cm^{-1}. At higher energy, two characteristic negative bands are observed between 23 000 and 28 000 cm^{-1} in the MCD spectra of **4** (bands 3 and 4). The corresponding absorption bands have an ϵ of 500−1300 M^{-1} cm^{-1}. These features correspond to bands 5 and 6 of the hydrotris(pyrazolyl)borate complexes (vide supra) and, hence, are assigned to corresponding CT transitions. For complex **4**, an intense absorption is observed around 35 000 cm^{-1} (band 5) with an ϵ of ∼2000 M^{-1} cm^{-1}, which is assigned to a CT transition between copper(II) and the bis(pyrazolyl)methane ligand. Again, this is similar to the results for the hydrotris(pyrazolyl)borate complexes (here: band 7). For the nitrato complex [Cu(L1″)(η^1-NO_3)$_2$], this transition can probably be identified with band 4a, although the UV−vis assignments are complicated by the low quality of the mull spectra obtained for this compound. Importantly, neither the mull nor the KBr nor the solution data of [Cu(L1″)(η^1-NO_3)$_2$] show further bands between 35 000 and 42 000 cm^{-1}. Therefore, the feature at about 39000 cm^{-1} in complex **4** with an ϵ of ∼2500 M^{-1} cm^{-1} (band 6) is associated with a σ-CT transition involving nitrite and copper(II). This feature probably corresponds to band 6a in the MCD spectrum of **4**, whose position is uncertain due to the fact that the signal intensity becomes very low above 38 000 cm^{-1} in the MCD. All band positions from a simultaneous fit of the absorption and MCD data are given in Table 9.

Summary and Conclusions

The structural and spectroscopic studies on copper(II)−nitrito complexes using the related tripodal coligands tris(pyrazolyl)methane (L′) and hydrotris(pyrazolyl)borate (L^-) and dipodal bis(pyrazolyl)methane (L″) presented here allow for the determination of the properties of these systems as a function of the applied coligand. In the case of anionic hydrotris(pyrazolyl)borate complexes, one nitrite is bound in an η^2-O,O bidentate mode to the copper(II) center. There is an important difference between the complexes depending on whether there are sterically demanding pyrazolyl substituents present in the coligand or not.[33] Using the less

Table 9. Results of the Simultaneous Gaussian Fit of the Absorption and MCD Spectra for the Compounds [Cu(L1″)(η^1-ONO)$_2$] and [Cu(L1″)(η^1-NO$_3$)$_2$]

	[Cu(L1″)(η^1-ONO)$_2$] (**4**)					[Cu(L1″)(η^1-NO$_3$)$_2$] (**5**)				
band	ν_{max} (cm^{-1})	ϵ_{max} (M^{-1} cm^{-1})		$\Delta\epsilon$ [T^{-1}]	f [a]	ν_{max} (cm^{-1})	ϵ_{max} (M^{-1} cm^{-1})		$\Delta\epsilon$ [T^{-1}]	f [a]
	7507	6.5	Q[b]		0.0001					
1	**11 384**	40.8	Q[b]	13.7	0.0006	**12 631**	130.0	Q[b]	10.4	0.0022
2	**15 426**	110.8	Q[b]	−29.9	0.0019	**15 931**	108.3	Q[b]	−27.0	0.0017
2a	19 750	38.0	Q[b]	−1.9	0.0007					
3	**23 845**	535.7		−6.8	0.0127	**23 133**			−4.9	
4	**28 770**	1372.2[c]		−22.5	0.0419	**28 307**	(1399)	M[b]	−26.7	(0.031)
4a						32 380	(1167)	M[b]	−4.6	(0.025)
5	35 306	2312.5[c]			0.0650					
6a	37 050			5.1						
6	39 049	2451.0[c]			0.0445					

[a] f: Oscillator strength. [b] Q: fit of the solid-state UV−vis spectra; the other band positions are obtained from the low-temperature UV−vis spectra in KBr for [Cu(L1″)(η^1-ONO)$_2$]. For [Cu(L1″)(η^1-NO$_3$)$_2$], mulls have been used instead (labeled M) which, however, do not allow for an accurate determination of ϵ_{max}. [c] The intensity of these bands is probably overestimated due to the scattering background of the KBr disk that becomes significant at low wavelengths

demanding ligand L1$^-$, the nitrite binding mode is symmetric and from EPR, the complex has the usually observed $d_{x^2-y^2}$ ground state. However, the complex with the bulkier ligand L3$^-$ shows an asymmetric binding of nitrite and a d_{z^2} ground state. Whereas this change of the ground state is nicely reflected by the EPR spectra, the vibrational properties of the complexes are hardly affected. This is a very good example on how second coordination sphere effects can influence the binding properties of a ligand and, this way, change the electronic structure of the resulting complex.[21b] In this case, a small change in the bulkiness of the coligand leads to a significant alteration of the properties of the metal site. In correlation with DFT calculations, we have reassigned the vibrational spectra of O-coordinated nitrite. Whereas in the previous studies it was always assumed that the asymmetric N−O stretch of nitrite is higher in energy than the corresponding symmetric combination, we were able to show that this is not the case. In fact, in complexes **1** and **2**, ν_s(N−O) is observed in the 1250−1300 cm^{-1} region, whereas ν_{as}(N−O) appears below 1200 cm^{-1}. Comparison of the absorption and MCD spectra of the nitrito complexes **1** and **2** with the data obtained for corresponding nitrato compounds shows that there is no CT transition of considerable intensity between nitrite and copper(II) present in the visible region of the electronic spectra. The observed weak CT bands around 400−500 nm of these compounds are most likely identified as pyrazole-π to Cu(II) (SOMO) transitions. In general, the optical spectra of the nitrito and nitrato compounds resemble the pattern of what has been termed 'normal' copper(II) complexes, where the d−d transitions occur at lowest energy, followed by weak π-CT in the visible region, and more intense σ-CT at high energy.[38] The assignments presented here are also in agreement with MCD data obtained on [Cu{HB(3-*t*-Bupz)$_3$}X] (X = Cl$^-$, CF$_3$SO$_3^-$, etc.) complexes,[17,39] but in these cases no detailed assignments of the optical spectra have been given. The difference in the coordination geometries between **1** (square pyramidal) and **2** (distorted trigonal pyramidal) is reflected by the four d−d transitions, which are present between roughly 7000 and 15 000 cm^{-1} in the optical spectra. Using DFT calculations, the different coordination isomers of nitrite to copper have also been investigated. Importantly, O- and N-coordination are practically isoenergetic for Cu(I). In the case of Cu(II), O-coordination is favorable by 5−6 kcal/mol. This not only explains why this is the preferred coordination geometry of nitrite to Cu(II) but also implies that N-coordination might be accessible with the right coligand.

In comparison to the crystal structure of Cu^{II}NIR soaked with nitrite,[7] the obtained coordination modes of nitrite in complexes **1** and **2** are different. The dihedral angles between the plane defined by the nitrogen and the two oxygen atoms and the plane defined by the two oxygen atoms and copper are 75 deg for CuNIR but only 2.3 deg for **1** and 0.1 deg for **2**. This difference relates to the weaker coordination of the NO_2^- ion in NIR as evident from the larger Cu−O(nitrite) distances, which, in turn, are due to the presence of a hydrogen bond between nitrite and Asp98 ('third' coordination sphere effects).

Applying the neutral tri- and dipodal ligands L′ and L″ leads to the coordination of two nitrite molecules to the copper(II) center in contrast to the hydrotris(pyrazolyl)borate complexes. This again demonstrates that the total charge of a ligand set, even if the charge carrier is quite far away from the metal site, is one of the most important second coordination sphere parameters with respect to influencing the coordination properties of the central metal.[21b] This, of course, especially applies to charged ligands like nitrite (and similarly, nitrate, chloride, etc.). In the case of L″, both nitrite ligands are monodentate η^1-O coordinated as evident from the crystal structure of **4**. The vibrational spectra show an interesting coupling scheme of the four local N−O vibrations where coupling between the equivalent N−O coordinates of different nitrite ligands dominates. The corresponding N−O stretches are identified at 1346/1325 and 1176 cm^{-1} in the spectra. Importantly, complex **4** is effectively four-coordinate (distorted square-planar). This is reflected by the MCD spectra showing a pseudo-**A** signal in the low-energy region, which corresponds to the Cu-d_{xz} to Cu-$d_{x^2-y^2}$ and Cu-d_{yz} to

(38) Solomon, E. I.; Szilagyi, R. K.; DeBeer George, S.; Basumallick, L. *Chem. Rev.* **2004**, *104*, 419−458.
(39) Tolman, W. B.; Carrier, S. M.; Ruggiero, C. E.; Antholine, W. E.; Whittaker, J. W. In *Bioinorganic Chemistry of Copper*; Karlin, K. D., Tyeklár, Z., Eds.; Chapman & Hall: New York, 1993.

Cu-$d_{x^2-y^2}$ transitions. The remaining two d−d transitions are located at lower energy. Again, no CT transition between copper(II) and nitrite is noticeable in this case in the UV−vis region, as can be seen by comparison with the optical spectra of the corresponding nitrato complex **5**. Finally, applying tripodal L′, a very special coordination of NO_2^- is observed: whereas one ligand shows the usual η^1-O binding, the second nitrite is N-coordinated. This mixed O/N coordination of two nitrites to copper(II) is unusual and has only been observed for a few compounds before.[36] Taken together, these crystal structures show that, depending on the applied coligand, the O-coordinated NO_2^- in such a case can either be mono- or bidentate. The mixed O/N binding mode of nitrite is reflected by the vibrational spectra of **3** showing the corresponding $\nu_{as}{}^{N}$(N−O) mode of N-coordinated NO_2^- at 1402 cm^{-1}, which is distinctively higher in frequency than observed for O-coordinated NO_2^-. Vice versa, the corresponding Cu−N stretch is found at 223 cm^{-1}, which is distinctively lower in energy than what is observed for the Cu−O stretch in the O-coordinated case. Importantly, *these vibrational features can actually be considered the best spectroscopic 'footprint' for N-coordination of nitrite to Cu(II)*. Further evidence is provided by the electronic spectra of **3**, which show an additional broad band around 300−330 nm in the UV region that might be attributable to a nitrite to copper(II) CT transition. However, the optical spectra of the corresponding nitrato complex are unreliable and, hence, do not provide further support for this conclusion. In addition, TD-DFT calculations do not reproduce the spectral features well in this energy region and cannot assist with the assignments. Hence, based on these data, no final conclusion about the nature of the UV spectroscopic features of **3** is possible. Finally, a special property of the d orbital based SOMO in N-coordinated nitrito complexes is that it shows a strong (antibonding) admixture of the σ-HOMO of the nitrite ligand (cf. Figure 5), leading to a large nitrite character of the SOMO of the complex. This creates spin density on the N-coordinated nitrite (about 0.4 in the calculation) and especially on the coordinated nitrogen itself. This is not observed for O-bound nitrite and indicates that N-bound nitrite exhibits a stronger oxidation upon coordination than the O-bound isomer.

In summary, these results demonstrate that there is a significant difference in the electronic structures of N- vs O-coordinated nitrite as reflected by the vibrational properties and that the coordination mode of the NO_2^- ligand itself critically depends on the nature of the coligand(s).[40] In future studies, we will use second coordination sphere effects by adjusting the pyrazolyl substituents to obtain additional N-coordinated nitrito complexes of copper(II) to further study their electronic structures in more detail.

Acknowledgment. This research was supported by the Fonds der Chemischen Industrie (N.L.), the Japan Society for the Promotion of Science Grant (Nos. 13555257, 14350471, and 17359943) (K.F.), and the Tokuyama Science Foundation (K.F.).

Supporting Information Available: Figures of vibrational and MCD spectra of additional nitrito and nitrato complexes, calculated absorption spectrum of **1d**, and crystallographic data in CIF format of **1**, **2**, **4**, and **5**. This material is available free of charge via the Internet at http://pubs.acs.org. Crystallographic data have been deposited at the CCDC, 12 Union Road, Cambridge CB2 1EZ, U.K., and copies can be obtained on request, free of charge, by quoting the publication citation and the deposition numbers: **1**, 611029; **2**, 611030; **4**, 611031; and **5**, 611032.

IC0619355

(40) We have not obtained any charged complexes such as [Cu(L1 or L3)(ONO)$(NO_2)]^-$ or [Cu(L1′)(ONO)$]^+$ in this reaction. Therefore, using charged ligands is a very useful strategy for controlling the coordination number of a rather weak ligand in a transition metal complex (using nonpolar solvents).